universe

MDPI

Article

The Evolution of Galaxies and Clusters at High Spatial Resolution with Advanced X-ray Imaging Satellite (AXIS)

Helen R. Russell [1,*], Laura A. Lopez [2], Steven W. Allen [3,4,5], George Chartas [6], Prakriti Pal Choudhury [7,8], Renato A. Dupke [9,10], Andrew C. Fabian [7], Anthony M. Flores [3,4], Kristen Garofali [11], Edmund Hodges-Kluck [11], Michael J. Koss [12], Lauranne Lanz [13], Bret D. Lehmer [14], Jiang-Tao Li [15], W. Peter Maksym [16,17], Adam B. Mantz [4], Michael McDonald [18,19], Eric D. Miller [19], Richard F. Mushotzky [20], Yu Qiu [21,22], Christopher S. Reynolds [20,23], Francesco Tombesi [24], Paolo Tozzi [25], Anna Trindade-Falcão [16], Stephen A. Walker [26], Ka-Wah Wong [27], Mihoko Yukita [11] and Congyao Zhang [28]

1 School of Physics & Astronomy, University of Nottingham, University Park, Nottingham NG7 2RD, UK
2 Department of Astronomy, The Ohio State University, 140 W. 18th Ave., Columbus, OH 43210, USA; lopez.513@osu.edu
3 Department of Physics, Stanford University, 382 Via Pueblo Mall, Stanford, CA 94305, USA; swa@stanford.edu (S.W.A.); aflores7@stanford.edu (A.M.F.)
4 Kavli Institute for Particle Astrophysics and Cosmology, Stanford University, 452 Lomita Mall, Stanford, CA 94305, USA; amantz@stanford.edu
5 SLAC National Accelerator Laboratory, 2575 Sand Hill Road, Menlo Park, CA 94025, USA
6 Department of Physics and Astronomy, College of Charleston, Charleston, SC 29424, USA; chartasg@cofc.edu
7 Institute of Astronomy, University of Cambridge, Madingley Road, Cambridge CB3 0HA, UK; prakriti.palchoudhury@physics.ox.ac.uk (P.P.C.); acf@ast.cam.ac.uk (A.C.F.)
8 Clarendon Laboratory, University of Oxford, Parks Rd, Oxford OX1 3PU, UK
9 Department of Astronomy, University of Michigan, 1085 South University Ave., Ann Arbor, MI 48109, USA; rdupke@umich.edu
10 Observatório Nacional, Rua Gal. José Cristino 77, Bairro Imperial de São Cristóvão, Rio de Janeiro 20921-400, Brazil
11 NASA/Goddard Space Flight Center, Greenbelt, MD 20771, USA; kristen.garofali@nasa.gov (K.G.); edmund.hodges-kluck@nasa.gov (E.H.-K.); myukita1@jhu.edu (M.Y.)
12 Eureka Scientific, 2452 Delmer Street Suite 100, Oakland, CA 94602, USA; mike.koss@eurekasci.com
13 Department of Physics, The College of New Jersey, Ewing, NJ 08628, USA; lanzl@tcnj.edu
14 Department of Physics, University of Arkansas, Fayetteville, AR 72701, USA; lehmer@uark.edu
15 Purple Mountain Observatory, Chinese Academy of Sciences, 10 Yuanhua Road, Nanjing 210023, China; pandataotao@gmail.com
16 Center for Astrophysics | Harvard & Smithsonian, 60 Garden St., Cambridge, MA 02138, USA; walter.maksym@cfa.harvard.edu (W.P.M.); anna.trindade_falcao@cfa.harvard.edu (A.T.-F.)
17 NASA Marshall Space Flight Center, Huntsville, AL 35812, USA
18 Department of Physics, Massachusetts Institute of Technology, Cambridge, MA 02139, USA; mcdonald@space.mit.edu
19 Kavli Institute for Astrophysics and Space Research, Massachusetts Institute of Technology, Cambridge, MA 02139, USA; milleric@mit.edu
20 Department of Astronomy, University of Maryland, College Park, MD 20742, USA; rmushotz@umd.edu (R.F.M.); creynold@umd.edu (C.S.R.)
21 Institute for Advanced Study in Physics, Zhejiang University, Hangzhou 310058, China; yuqiu@pku.edu.cn
22 Kavli Institute for Astronomy and Astrophysics, Peking University, Beijing 100871, China
23 Joint Space-Science Institute (JSI), College Park, MD 20742, USA
24 Dipartimento di Fisica, Università degli Studi di Roma "Tor Vergata", Via della Ricerca Scientifica 1, 00133 Roma, Italy; francesco.tombesi@roma2.infn.it
25 INAF—Osservatorio Astrofisico di Arcetri, Largo E. Fermi, 50122 Firenze, Italy; paolo.tozzi@inaf.it
26 Department of Physics and Astronomy, University of Alabama in Huntsville, Huntsville, AL 35899, USA; saw0041@uah.edu
27 Department of Physics, SUNY Brockport, Brockport, NY 14420, USA; kwong@brockport.edu
28 Department of Astronomy and Astrophysics, The University of Chicago, Chicago, IL 60637, USA; cyzhang@astro.uchicago.edu
* Correspondence: helen.russell@nottingham.ac.uk

Abstract: Stellar and black hole feedback heat and disperse surrounding cold gas clouds, launching gas flows off circumnuclear and galactic disks, producing a dynamic interstellar medium. On large

check for updates

Citation: Russell, H.R.; Lopez, L.A.; Allen, S.W.; Chartas, G.; Choudhury, P.P.; Dupke, R.A.; Fabian, A.C.; Flores, A.M.; Garofali, K.; Hodges-Kluck, E.; et al. The Evolution of Galaxies and Clusters at High Spatial Resolution with Advanced X-ray Imaging Satellite (AXIS). *Universe* **2024**, *10*, 273. https://doi.org/10.3390/universe10070273

Academic Editor: Marc S. Seigar

Received: 26 April 2024
Revised: 6 June 2024
Accepted: 12 June 2024
Published: 25 June 2024

scales bordering the cosmic web, feedback drives enriched gas out of galaxies and groups, seeding the intergalactic medium with heavy elements. In this way, feedback shapes galaxy evolution by shutting down star formation and ultimately curtailing the growth of structure after the peak at redshift 2–3. To understand the complex interplay between gravity and feedback, we must resolve both the key physics within galaxies and map the impact of these processes over large scales, out into the cosmic web. The Advanced X-ray Imaging Satellite (AXIS) is a proposed X-ray probe mission for the 2030s with arcsecond spatial resolution, large effective area, and low background. AXIS will untangle the interactions of winds, radiation, jets, and supernovae with the surrounding interstellar medium across the wide range of mass scales and large volumes driving galaxy evolution and trace the establishment of feedback back to the main event at cosmic noon. This white paper is part of a series commissioned for the AXIS Probe mission concept; additional AXIS white papers can be found at the AXIS website.

Keywords: X-rays; instrumentation; galaxies; clusters; feedback

1. Introduction

Galaxies form and evolve through a vigorous cosmic struggle. The inexorable pull of gravity drives the assembly of galaxies by drawing primordial gas into dark matter halos and collapsing cold clouds into stars. At most, twenty percent of baryons are converted into stars (e.g., [1]). This inexplicable inefficiency across the galaxy mass scale is the result of high-energy processes around stars and supermassive black holes. Stellar feedback, via stellar winds and supernovae, heats and disperses cold gas clouds and collectively inflates large gas bubbles that lift hot gas and metals into galactic halos (for reviews, see [2,3]). In massive galaxies, more powerful feedback from active galactic nuclei (AGN), in the form of radiation, winds and relativistic jets, drives large outflows, suppresses the cooling of hot atmospheres, and produces a correlative slowing of black hole activity [4]. Feedback indelibly shapes galaxy evolution on all scales of the galaxy mass function, back to the peak of galaxy growth at $z \sim 2$ and beyond.

X-ray observations reveal the key interactions on all spatial scales: the acceleration of winds and jets close to black holes, the impact zones where stellar winds, supernovae, AGN winds, and jets meet the interstellar medium(ISM), and the distribution of energy and metal-rich gas across galaxy halos. Arcsecond spatial resolution is essential for disentangling the complex interactions of winds, radiation, jets, and supernovae with the surrounding gas. However, only when combined with high throughput can the key scales of individual HII regions, star clusters, wind shocks, and jet-blown bubbles be reached across the galaxy population, tracing the establishment of feedback back to the main event at cosmic noon. AXIS now capitalizes on the key technological advance of precision focusing with lightweight X-ray mirrors to deliver 1.5 arcsec spatial resolution on-axis, 1.6 arcsec on average across the 24 arcmin field of view, and a factor of ~ 10 increase in the collecting area over existing facilities [5]. AXIS will answer major questions on feedback, including the following:

- How do star-forming structures shape the ISM? What are the conditions for breakout or outflow?
- How do AGN winds and jets inject energy and drive outflows in individual galaxies?
- How and when did AGN feedback begin to shape the evolution of galaxy clusters and groups?
- How and when did the hot and diffuse universe become enriched with heavy elements?

Furthermore, in combination with the low-particle background of a low-inclination low Earth orbit, AXIS will unveil the faint and diffuse X-ray universe: the remarkable interconnected gas flows that comprise the cosmic web, giant filaments that feed cluster assembly, and the missing baryons in the circumgalactic medium (CGM, see [6]).

In this white paper, we discuss how AXIS will transform our understanding of all aspects of feedback in galaxies, a main science driver of the mission, and we present the far wider impact that AXIS will precipitate across all areas of galaxy formation and evolution, which will be realized in >70% of the general observer time.

2. Stellar Feedback in Nearby Galaxies

Over the past decade, observational and theoretical investigations have revealed that the large-scale behavior of galaxies (e.g., the shape and structure of galaxies, and the rate and efficiency of star formation) emerges from local phenomena, particularly stellar feedback [7]. The injection of energy and momentum by stars has a profound influence on their surroundings. For example, stellar winds and supernovae from massive star clusters inflate bubbles that disrupt natal clouds [8], triggering star formation on their periphery and dispersing gas and metals that become fodder for the next generation of stars [9]. Collections of these bubbles build on each other, and in the extreme cases of starburst galaxies, form superheated gas that can drive galactic winds that eject much of the ISM gas into galactic halos [2].

Stellar feedback is often cited as one of the biggest uncertainties in star and galaxy formation (e.g., [7,10]), stemming from the need to constrain how the energy and momentum of star clusters is partitioned and coupled to the ISM. Feedback operates through several channels (e.g., photoionization, radiation, stellar winds, supernovae, and cosmic rays), and their effectiveness and impact vary, depending on the star cluster mass, age, metallicity, and environment. An accurate energetics inventory that measures feedback efficiency is crucial to understand galactic ecosystems. This endeavor necessitates a multi-wavelength perspective to connect cluster stars (UV, optical, and infrared) to ionized gas clouds (HII regions, X-ray, UV, and optical) and the surrounding ISM (mm, radio, and infrared).

X-ray observations are a critical missing piece and are essential to quantitatively measure the energetics because they trace the internal energy remaining in the hot gas. How and where this energy is lost remains an open question (e.g., [11,12]). However, HII regions have sizes of $1-200$ pc and typical luminosities of $L_X = 10^{32} - 10^{37}$ erg s^{-1}, largely inaccessible by modern X-ray facilities even in the Local Group. To date, only the brightest ($>10^{37}$ erg s^{-1}) tens of sources in the Local Group have been studied because *Chandra* lacks the sensitivity to detect fainter sources and XMM-*Newton* cannot resolve them spatially.

The high spatial resolution and large, soft X-ray collecting area of AXIS will enable the first representative inventory of the X-ray properties of individual star-forming regions ($1-10$ arcsec scales) in nearby (<7 Mpc) galaxies (Figure 1). AXIS will measure the X-ray signatures (e.g., temperature, density, and luminosity) of >5000 star clusters down to $L_X \sim 10^{34}$ erg s^{-1} in these galaxies, sufficient to detect the X-ray counterparts of star cluster populations and to produce the first-ever X-ray luminosity function of this population. Nearby targets offer a wide range in parameter space to quantify feedback efficiency via, for example, the outflow mass-loading factor and the stellar winds and supernovae thermalization efficiency constrained from the hot gas properties. These properties will be determined as a function of cluster mass, age, metallicity, galactocentric radius, and star cluster concentration, which are necessary inputs to test star and galaxy formation models.

X-rays are a longstanding missing piece in the puzzle of stellar feedback and its role in galactic ecosystems. By measuring the internal energy of a vast range of star clusters in nearby galaxies for the first time as part of the core science program, AXIS will finally provide the long-sought quantification of how hot gas from stellar winds and supernovae, X-ray binaries, and cosmic rays regulate star formation and shape galaxies.

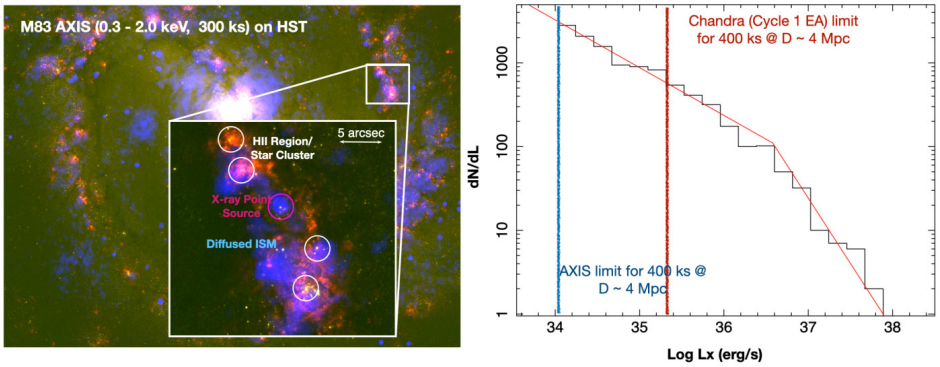

Figure 1. AXIS 300 ks simulation of the soft-band (0.3–2 keV) image of the spiral galaxy M83. X-ray binaries and diffuse hot gas are apparent, occupying the star-forming regions and inflating bubbles through the collective influence of supernovae and stellar winds. With AXIS sensitivity and spatial resolution, spectro-imaging analyses across arcsecond (10–30 pc) scales are possible. Right: A sharp, sensitive survey will definitively measure the luminosity function of >5000 star clusters down to below the "knee" in the Hα luminosity function. *Chandra* is not able to achieve these depths in multiple Ms even with capabilities at launch.

3. Black Hole Feedback: Quasar Mode

3.1. Quasar-Mode Feedback in Nearby Galaxies

Even though the central SMBH has a mass of only $\sim 0.1\%$ of its host galaxy, the enormous radiative and mechanical energy released as it grows (and shines as an AGN) can slow or completely suspend the entire galaxy's growth (for reviews see [4,13]). Now included as standard physics in simulations of structure formation, this mechanism may be able to transform gas-rich, star-forming progenitors into 'red and dead' ellipticals and imprint the observed strong correlation between black hole mass and galaxy bulge velocity dispersion [14–16]. The majority of black hole growth occurs during phases of a high-accretion radiative/quasar mode, where intense radiation and high-velocity winds off the accretion disk heat, ionize, and expel gas from the surrounding ISM [17–20]. However, estimates of the energy and momentum input vary widely, and the necessary coupling to kpc-scale cold gas clouds is still far from being fully understood.

Spatially resolved spectroscopy on scales of hundreds of parsecs (arcsec scales) is required to resolve the intricate structure of shocks, and ionization cones, to map the resulting transitions in the hot gas properties, and to thereby measure the energy transmitted to the surrounding ISM. With an order of magnitude increase in the soft X-ray effective area, AXIS will dramatically extend our reach beyond the few brightest, most massive systems to cover extensive samples of individual galaxies in the local universe and to develop physical models for the unresolved quasar feedback at the peak epochs of galaxy and black hole growth at much higher cosmological redshifts ($z > 2$).

AXIS observations of nearby Seyferts will map the impact zones where winds from the luminous AGN first meet the ISM (Figure 2). Outflow velocities at hundreds of parsec scales are typically $\sim$1000 km s^{-1}, for which the characteristic interaction energies are 1 keV and require X-ray observations. Soft X-ray bright knots and arcs result from a complex mixture of photoionization and thermal shock emission (e.g., [21–23]), which AXIS will disentangle with multi-component spectral models on arcsec scales and measurements of multiple high-ionization species to break degeneracies. With its unprecedented large effective area, AXIS will detect very low surface brightness components to test complex shock heating models, such as "slow cooling" where the gas is strongly heated, cannot cool efficiently, and produces disconnected arcs of X-ray emission, as the energy is dissipated far beyond the deceleration point (e.g., [24]). AXIS could rapidly observe large samples in the GO phase and cover a wide range of AGN luminosities, accretion rates, and galaxy masses. AXIS will then quantify the thermal power injected into the ISM as a fraction of the AGN bolometric luminosity and test different feedback models. The strong coupling

of the radiative energy would imply so-called simple AGN feedback, where a supersonic pressure or momentum-driven outflow off the accretion disk propagates to large scales. Weaker coupling would instead signify a two-stage mechanism, where radiative pressure drives a weak wind in the hot ISM, and secondary effects, such as the radiative effects of dust absorption and ionization, act on cold gas at large scales [25].

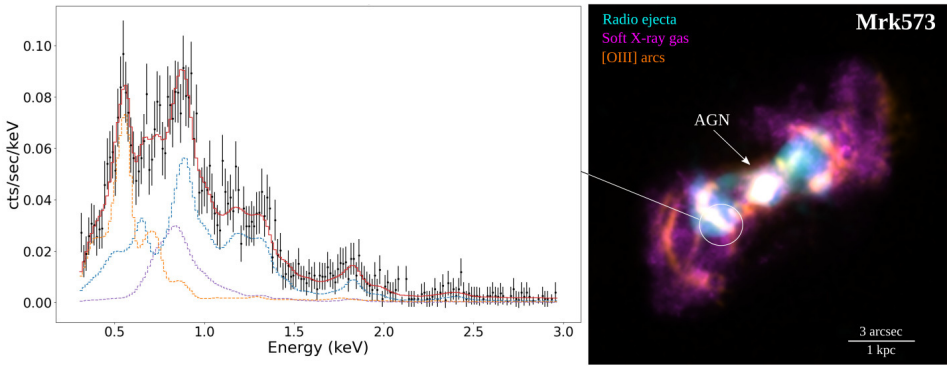

Figure 2. Composite image of the Seyfert galaxy Mrk573 comprising a PSF-deconvolved *Chandra* image, radio VLA 6 cm emission from the radio jets and HST [O III] emission (adapted from [26] with permission, Credit: X-ray: NASA/CXC/SAO/A.Paggi et al; Optical: NASA/STScI; Radio: NSF/NRAO/VLA). Simulated AXIS spectrum (150 ks) for the region shown. The best-fit model has one thermal component (purple line) and two photoionization components (blue and orange lines). The total model is shown by the red line.

3.2. Quasar Feedback at High Cosmological Redshifts

The observed evolution of the stellar mass of galaxies (e.g., [27]) indicates that approximately 75% of the stellar mass had already formed before $z \sim 1.3$. It is therefore important to determine the energetics and morphology of multi-phase outflows/winds at high redshift, near the peak of AGN and star formation activity. One prediction of the numerical models of ultrafast outflows (UFOs) is that they interact with the ISM, producing shocks and extended X-ray emission at the shock front (e.g., [28,29]). The extent of the shocked ISM gas is predicted to be of the order of $\sim 0.1 - 1$ kpc. At $z = 2$; this corresponds to a range of angular sizes of $0.01 - 0.1$ arcsec that cannot be resolved by any current X-ray telescope. A direct detection of the interaction of a small-scale UFO originating at 10–100 r_g, where $r_g = GM_{BH}/c^2$, with kpc-scale gas would provide confirmation that UFOs transfer a significant amount of their energy to the host galaxy and are thus an important component of galaxy feedback.

When gravitationally lensed, a compact quasar source forms multiple images whilst any extended emission around the quasar forms a ring (i.e., Einstein ring) that connects the individual images. A technique that has been successfully employed to resolve extended optical and IR emission around quasars involves lens modeling the Einstein rings of gravitationally lensed quasars. Finding lensed extended emission is easier than finding unlensed extended emission because the lens magnification enormously reduces the contrast between the extended emission and the central quasar [30]. The detections of X-ray Einstein rings associated with UFOs in distant lensed quasars are rare due to their X-ray weakness and the limited number of known lensed quasars with relativistic outflows [31]. The detection of both the UFO from the spectra of the lensed images and the extended emission from the shock can only be accomplished with an X-ray telescope with a PSF of the order of 1 arcsec (required to resolve the lensed images and Einstein ring) and an effective area of about >10 times *Chandra* (required to obtain high signal-to-noise UFO and shocked ISM spectra). AXIS is the only proposed X-ray probe mission that meets these requirements.

A hint of the detection of both a UFO and an Einstein ring is provided in the *Chandra* observations of the lensed quasar PG 1115+080 [32]. PG 1115+080 is a quadruply lensed quasar containing a powerful UFO ($v \sim 0.4$c). Our preliminary spatial analysis of the

available *Chandra* observations of PG1115+080 shows hints of a partial X-ray Einstein ring. In Figure 3, we show the deconvolved *Chandra* image obtained by stacking all available *Chandra* observations (total exposure time of 173 ks). The extended emission forming a partial Einstein ring is visible in both the stacked observation and in a single 30 ks observation of PG115+080. The *Chandra* spectrum of the partial Einstein ring is also shown in Figure 3. An acceptable spectral model includes a plane-parallel shock plasma model and an absorbed power-law model. Due to the low signal-to-noise ratio, however, a model that only includes an absorbed power law also provides a satisfactory fit to the data. We simulated an AXIS spectrum with a matching exposure time (173 ks) using the best-fit model to the *Chandra* spectrum of the partial Einstein ring (Figure 3). The simulated AXIS observation of PG1115+080 shows that we will unambiguously detect the presence of shocked emission from the interaction of the UFO with the ISM.

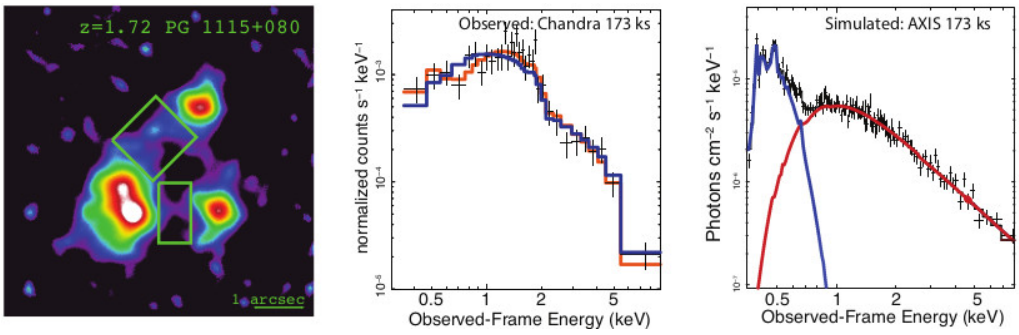

Figure 3. (**Left**): A deconvolved *Chandra* image obtained by stacking all available observations of PG1115+080 (total exposure time of 173 ks). A partial X-ray Einstein ring is resolved between lensed images. (**Center**): The stacked 173 ks *Chandra* spectrum extracted from the regions (**left**) covering the partial X-ray Einstein ring. A model that includes a plane-parallel shock plasma component plus a power-law component is shown in red. The spectrum can be equivalently fit by only a power-law model (blue). (**Right**): A simulated 173 ks unfolded AXIS spectrum of the partial X-ray Einstein ring clearly resolves the shocked plasma component (blue) from the power-law component (red).

There is an important synergy between AXIS and other multi-wavelength observatories that will improve our understanding of galaxy feedback through multi-phase winds. Spectra and images from mm observatories (e.g., ALMA) will be used to determine the properties of the macro-scale winds. Numerical models of UFOs (e.g., [28,29]) predict that they drive powerful winds that heat and expel cold gas from the galaxy on larger scales. At present, there are few examples where the momentum flux of the AGN wind can be linked to a large-scale molecular outflow, but a combination of AXIS and ALMA can increase the sample and allow us to test models of this process. The Vera C. Rubin Observatory is predicted to discover >10,000 gravitationally lensed quasars, most of which will be resolved with AXIS ([33], see Figure 4). The planned observing window of AXIS (∼2032–2037) will overlap with the multi-band photometric optical surveys of Rubin (∼ 2024–2034), GAIA, and EUCLID. The eROSITA all-sky survey will provide the X-ray fluxes of the lensed quasars discovered by Rubin and other surveys (J-PAS, Pan-STARRS1, DESI legacy, and Dark Energy Survey) but cannot resolve the lensed images or extended emission. AXIS will target lensed systems that are sufficiently X-ray bright and detect UFOs and Einstein rings.

AXIS observations of a sample of high-z lensed quasars will allow us to study both the central drivers of galaxy growth at the smallest scales (1–100 r_g) and the interaction of the winds with the ISM at the mesoscale ($\sim$ pc $-$ kpc).

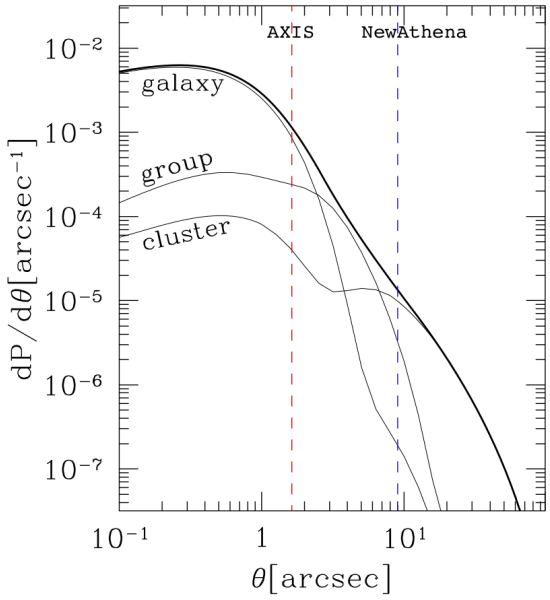

Figure 4. The distribution of lens image separations for three different lens types − galaxy, group, and cluster scales − predicted by a halo model. The total distribution is shown by the thick line. The vertical lines represent the current best estimate half-power diameters of AXIS and Athena.

4. Black Hole Feedback: Radio Mode

4.1. Radio-Mode Feedback in Galaxies

Powerful radio jets are a means by which AGN exert influence on their host galaxies but how they are able to provide steady, distributed, and self-regulated heating to galaxy and cluster environments is still not well understood (see [13,34] for reviews). Mechanical- or radio-mode feedback typically occurs when accretion is happening at low rates ($\lesssim 1\%$ of the Eddington rate), enabling this mode to be active for longer periods than intense quasar mode feedback (see Section 3.1). Radio-mode AGN have primarily been studied in massive systems, where they must efficiently couple to their surrounding hot X-ray atmospheres to suppress cooling and maintain low levels of star formation at late times. The physical processes by which the energy and momentum are transferred to cooling and star-forming gas, distributed on galaxy scales, and how these mechanisms scale with host mass remain unknown.

Spatially resolved spectroscopy with high angular resolution is critical for resolving and characterizing extended diffuse emission and differentiating between feedback from nuclear star clusters and star formation and feedback from the AGN including via small-scale jets. As jets encounter the ISM, they can shock some of this gas to a range of temperatures, producing emission in the mid-infrared (e.g., [35]) and X-ray bands (e.g., [36]). The high throughput of AXIS coupled to the arcsecond spatial resolution will be key in resolving the structure and properties of the hot gas for comparison with warm gas mid-IR and near-IR tracers mapped by JWST and Roman, enabling us to trace the processes by which energy is deposited into the ISM from radio jets. Figure 5 shows a comparison of *Chandra* observations from Cycle 11 and Cycle 18 with an AXIS spectrum of the same outflow region in NGC 1266. The typical temperature of galactic hot atmospheres lies below 1 keV and the dramatic loss of *Chandra* ACIS soft response (currently only 8 cm^2 at 0.5 keV) has long placed these targets out of reach (e.g., [37]). With an effective area more than 400 times *Chandra* ACIS at 0.5 keV, AXIS will allow detailed studies of the mechanical processes by which AGN impart energy to their host galaxies and crucially widen our view from individual investigations of only the brightest sources to statistically important samples.

On larger scales of a few to tens of kpc (arcsec to tens of arcsec), jets inflate huge bubbles of radio-emitting plasma and couple very efficiently to the volume-filling hot CGM (e.g., [38–40]).

Our current understanding is almost entirely shaped by deep *Chandra* observations of the nearest, richest cluster atmospheres (e.g., Perseus, [39]; M87, [41]; Centaurus, [42]; and Abell 2052, [43]). Although remarkable, these systems are clearly unrepresentative of the wider galaxy population driving the slowdown in star formation at low redshift. *Chandra* observations of the brightest ellipticals indicate analogous jet interactions with the galaxy's hot atmosphere [44,45] but are severely limited by the loss of the ACIS effective area at low energies. The expansive soft response of AXIS will enable Perseus-like studies for numerous systems in the nearby universe to determine if feedback stabilizes cooling in all nearby massive galaxies, whether cluster processes scale down, and what the dominant mechanism is for distributing and dissipating energy throughout the galaxy's hot atmosphere. Figure 5 (left) shows all galaxies in the ATLAS^{3D} sample with *Chandra* observations [46] measuring the global properties of the hot atmosphere. With at least 10,000 counts per target in a large sample with AXIS, we will identify cavities, measure the gas properties in radial profiles, and calculate the energy input by the AGN. AXIS observations of massive ellipticals (Figure 6) will uncover additional pairs of relic bubbles from previous AGN outbursts to reveal the history of AGN activity, whether bubbles break up, merge or pile up at large radius, trace metal-rich, low entropy gas flows, and determine the implications for the distribution of the energy input by jets. In this way, for the first time, AXIS will reveal how feedback operates across the whole gamut of hot atmospheres from L* galaxies at 10^{12} $M_\odot$ to the richest clusters above 10^{15} $M_\odot$.

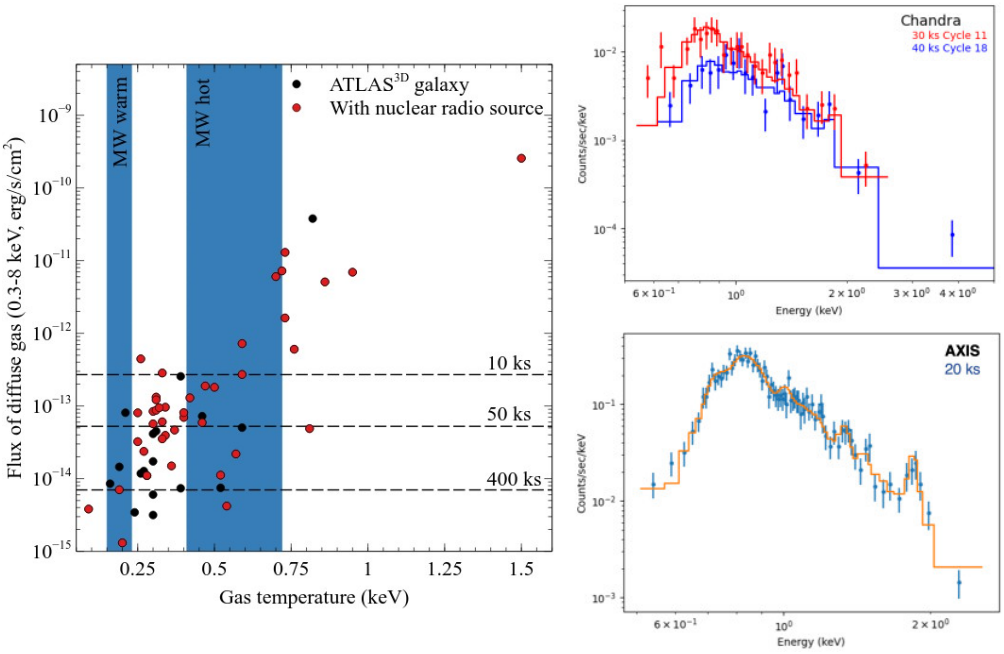

Figure 5. (**Left**): X-ray flux vs. gas temperature for galaxies in the ATLAS^{3D} sample [47] with *Chandra* observations [46]. AXIS exposure times to obtain >10,000 counts from the diffuse gas are shown for representative targets. Note that, given the low temperatures of these hot atmospheres, 10 ks with AXIS is equivalent to 250 ks with *Chandra* at launch and 2.5 Ms currently. Uncertainties on *Chandra's* global temperature measurements are not shown for clarity but are typically 15–80%. Galaxies with and without detected nuclear radio emission are shown by the red and black points, respectively [48]. The temperature components of the Milky Way's circumgalactic medium are shown for reference (e.g., [49]). (**Right**): *Chandra* (**upper**) and simulated AXIS spectra (**lower**) and best-fit models for NGC 1266, a post-starburst lenticular with a 6″ multi-phase nuclear outflow, showing the degradation of *Chandra*'s soft response and the benefit of the high effective area of AXIS. More than twice as many photons were collected in less than 1/7th of the exposure time.

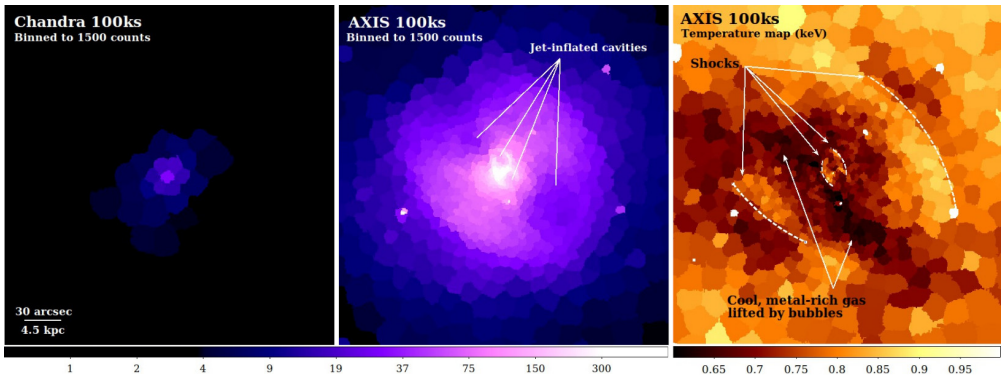

Figure 6. (**Left**,**Center**): *Chandra* (at launch) and AXIS-simulated images of AGN feedback in NGC 5813 (100 ks) with spatial binning for 1500 counts per region. Color bars are matched and units are counts arcsec^{-2}. The radio jet has carved out large cavities in the galaxy's hot atmosphere, which are visible in the AXIS simulation as depressions in the X-ray surface brightness. With 1500 counts per region, AXIS will map the gas properties on these spatial scales to an accuracy of a few percent points in temperature. The spatial bins are generated with the contour binning algorithm and group pixels with similar surface brightness [50]. All panels cover the same field of view. (**Right**): Simulated temperature map in keV for a 100 ks AXIS observation, which probes the thermodynamic properties on the scales of the bubble rims, shocks, and cool gas plumes [51,52].

4.2. Feedback in Galaxy Clusters

AGN feedback reaches far beyond the SMBH sphere of influence to interact with the multi-phase medium in and around galaxies. In galaxy clusters, where there is a concentration of hot gas pulled in by the dark matter halo, AGN feedback acts against gravity to shape the structure of the X-ray-emitting intracluster medium (ICM). Direct imaging of the ICM with X-ray facilities has proven fruitful in detecting imprints of AGN activity. For example, Chandra has detected the innermost cavities inflated by radio jets in numerous rich clusters and shown that the energy required to inflate them is sufficient to suppress the cooling of cluster atmospheres [34,53]). However, the physical mechanisms by which the jets heat the ICM or the residual gas cooling fuels the AGN remain unknown. Very deep *Chandra* observations of a few of the nearest clusters, such as Perseus, reveal highly structured networks of soft X-ray filaments, weak shocks, sound waves, turbulence, and numerous pairs of outer bubbles (for a review, see [13]). The AXIS angular resolution, soft response, and wide field of view are therefore essential to understand how the distribution, multi-temperature thermal state, and metallicity evolution of the plasma are influenced by AGN feedback in a wide range of clusters.

The cooling of the ICM in cool-core clusters is inextricably linked with AGN feedback (e.g., [54,55]). How the plasma cools and forms (sometimes star forming) cold filaments is still a highly debated topic, including theoretical models such as plasma thermal instability, the uplift of low-entropy gas by AGN-driven bubbles, and radiatively cooling AGN-driven outflows [56–61]. The AXIS soft response and spatial resolution are perfect for tracing the lowest energy plasma out of which these filaments form (Figure 7), potentially unveiling the fueling of the central AGN and the growth of the stellar component. When combined with optical and radio observations (such as SITELLE, MUSE, and ALMA) that capture the velocity distribution and turbulent structures of the cold gas [62,63]), AXIS will enable a comprehensive account for the continuous thermodynamical evolution of the plasma, and further reveal the role AGNs play in tightly controlling the growth of these elliptical galaxies.

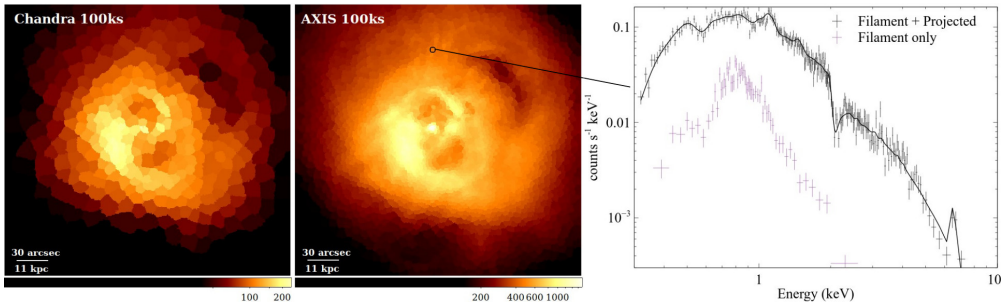

Figure 7. (**Left**): *Chandra* image of the Perseus cluster (100 ks at launch) with spatial binning for 7500 counts per region (color bar units counts arcsec^{-2}). (**Center**): AXIS simulated image of the Perseus cluster (100 ks) also binned for 7500 counts per region. (**Right**): AXIS simulated spectra for the region shown with a radius of 2.5 arcsec (factor of 10 reduction in spatial bin size compared to *Chandra*). The total spectrum and model are shown in black, and the intrinsic emission from a region of the soft X-ray filament (shown center, projected emission subtracted with a neighboring off-filament region, [64]) is shown in purple.

In the absence of AGN feedback, the properties of the ICM, such as temperature and density distribution, are determined primarily by the underlying gravity [65]. Detecting and characterizing property modifications associated with the activities of the AGN are therefore crucial in understanding how feedback energy is delivered to the surrounding medium. Measurements of shocks, cavities, and turbulence (e.g., [41,52,66]) in the plasma all require a large collecting area with arcsecond resolution. The AXIS advancement over existing X-ray imaging telescopes enables the detection of these features beyond the central tens of kpc. The combination of spatial resolution (providing detailed maps of the density and temperature structure) with velocity structure from future X-ray calorimeters (such as XRISM, HUBS, and Athena) is key to understanding how energy is transmitted to the ICM and distributed throughout the cluster core.

4.3. Hidden Cooling Flows in Clusters

The radiative cooling time at the center of the hot atmospheres of massive galaxies, groups and clusters can drop below 10 Myr. The observed mass cooling rate of this gas is very low and drops to near zero as the gas temperature falls below 0.4 keV [67–69]. Either AGN feedback is very tightly balanced as discussed in Sections 4.1 and 4.2, or the soft X-ray emission from cooling is somehow hidden from view, which is considered here. The gas in the centers of cool core clusters, groups, and elliptical galaxies is then cooling at significant rates of order 100, 10, and 1 $M_\odot$ yr^{-1}, respectively. As the gas cools below 1 keV in the central kpcs, it becomes entwined with the gas that has already cooled. It is hidden from direct detection by photoelectric absorption in the cold gas as revealed by a recent analysis of *XMM-Newton* RGS spectra [70].

The fate of the rapidly accumulating cold gas is unknown, but the observed metallicity peaks at about 10 kpc radius in nearby clusters indicate slow outflows of enriched gas from their centers. Some gas may, however, become ultra-cool at close to 3 K, fragment, and form low mass stars [70]. Some low-mass stars may be swallowed whole by the central black hole while emitting little radiation [71].

The high angular resolution and soft response of AXIS will enable detailed spatial and spectral mapping of these important regions, uncovering the workings of the innermost parts of the most massive galaxies in the universe (Figure 8).

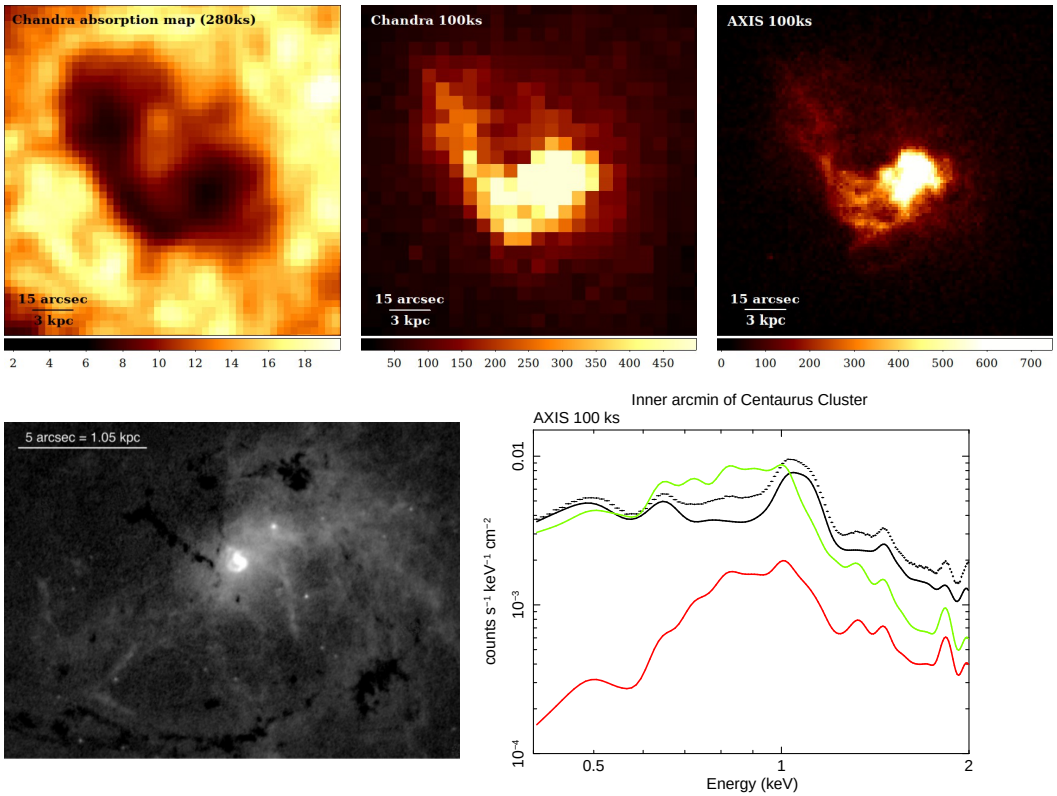

Figure 8. *Chandra* images, HST images and AXIS simulations of strong absorption at the center of the Centaurus cluster. Upper left: ratio of soft (0.5 − 0.7 keV) and mid-band (0.8 − 1.1 keV) *Chandra* images (280 ks taken 2000 − 2004) showing regions of strong absorption in the center of the Centaurus cluster. Upper center: 100 ks *Chandra* soft band counts image binned for >100 counts per pixel in regions of interest. Upper right: same as the center but for 100 ks with AXIS. Substantial expansion of the soft response with AXIS ensures over an order of magnitude improvement in resolution. Lower left: HST Hα image of the core of the nearby Centaurus cluster around its brightest cluster galaxy NGC 4696 [72]. Note the dusty filaments and emission clouds, all of which will absorb soft X-rays originating from this region. Lower right: simulated 100 ks AXIS spectrum of the inner arcmin diameter of NGC 4696. The green line shows a $15\,M_\odot\ yr^{-1}$ cooling flow, the red line similar but with a total intrinsic absorption of $1.6 \times 10^{22}\ cm^{-2}$ included to match the XMM RGS result [70]. The AXIS spectrum will vary between the green to below the red line depending on the absorption along a specific sightline, as on the left.

4.4. Inverse Compton Ghosts in the Deep X-ray Sky

Powerful jetted AGN feedback from isolated galaxies leads to giant double-lobed sources in the radio band. The energetic electrons in the lobes lose energy to inverse Compton scattering of the microwave background, the energy density ϵ_{cmb} of which grows with redshift z as $(1+z)^4$. The lifetime of an electron of the Lorentz factor γ scales as $1/(\gamma\epsilon_{cmb})$. Consequently, when the jets switch off, the radio emission, requiring $\gamma \sim 10^4 - 10^5$, dies away faster than the inverse Compton X-ray emission, which requires $\gamma \sim 10^3$. This results in a double-lobed inverse Compton ghost appearing in the soft X-ray band (its spectrum is likely steep). A candidate ghost was found in the 2 Ms *Chandra* Deep Field North, centered on the massive galaxy HDF 130 at $z = 1.99$ (Figure 9, see [73]). The lack of any such ghosts in the deeper *Chandra* Deep Field South is likely due to the lack of sensitivity to soft X-rays that developed due to the buildup of obscuring matter in the optical blocking filter on *Chandra's* ACIS detector. Such sources may have a higher space density than clusters at $z > 2$ and $L_X > 10^{44}$ erg s^{-1}.

Several other examples of jets with X-ray but not radio emission have been reported from the *Chandra* observations [74]. AXIS should detect many more with its capability to

map faint X-ray emission. The distribution with redshift and luminosity will provide a valuable guide to the importance and evolution of jetted feedback in isolated galaxies.

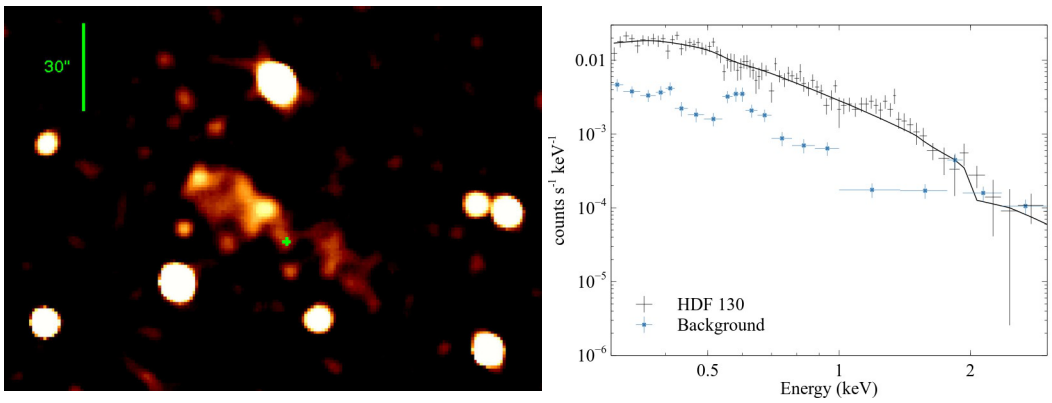

Figure 9. (**Left**): The extended X-ray emission around HDF 130 at $z = 1.99$ [73]. It is an inverse Compton ghost of a giant radio source in the *Chandra* Deep Field North (2 Ms). The *Chandra* spectrum for HDF 130 can be equivalently fit by power-law and thermal models. (**Right**): Simulated AXIS spectrum of HDF 130 in a 300 ks pointing from the AXIS Wide Survey. The AXIS simulated background (soft and non-X-ray background) and the best-fit power-law model with $\Gamma = 2.65 \pm 0.05$ and $\chi^2 = 80$ for 89 degrees of freedom (compared to $\chi^2 = 111$ for 89 degrees of freedom for a thermal model) are also shown.

5. The Integrated History of Feedback with High-z Clusters

5.1. Radio-Mode Feedback in High-z Clusters

Galaxy clusters are the pinnacle of hierarchical structure formation. As the most massive and largest virialized structures in the universe, clusters provide unique, high-density environments within which to study the physics of galaxy evolution [75,76]. Their deep gravitational potentials preserve the integrated history of generations of star formation and AGN feedback in the thermodynamic properties [77–79]. Powerful new surveys at millimeter (e.g., South Pole Telescope, Atacama Cosmology Telescope, Simons Observatory, and CMB-S4), optical/near-IR (e.g., Rubin, Roman, and Euclid), and soft X-ray wavelengths (eROSITA) are now set to expand, by orders of magnitude, the size of cluster catalogs (Figure 10). Critically, the new millimeter and optical/near-IR surveys will also reach much further in redshift, back to the epoch when these massive, virialized structures first formed. High-spatial-resolution X-ray follow-up observations of high redshift clusters will unfurl the complex interplay between gravity, star formation, and AGN feedback over their full history. However, such measurements lie beyond the reach of existing facilities: detailed studies with *Chandra* and *XMM-Newton* are restricted to $z < 1$, with only a handful of low S/N measurements for a few extreme systems that extend to $z \sim 1.5$. With its combination of high spatial resolution, expansive soft X-ray response, low instrumental background, and wide field of view, AXIS will transform our understanding of high redshift clusters, allowing us to observe their complete formation history, including the period of 'cosmic noon' ($z \sim 2 - 3$), when AGN and stellar activity within them are peaked.

AXIS guarantees that time observations will target the most massive, most luminous X-ray clusters discovered at redshifts $1.5 < z < 3$, resolving the AGN within them and measuring the density and temperature of the ICM, to a precision of better than 5% on spatial scales as small as 20 kpc. Such measurements, which also provide determinations of the pressure and entropy structure of the ICM, will reveal the evolving and cumulative impact of AGN feedback on its environments. For brighter targets, AXIS will also determine the instantaneous impact of this feedback manifested, for example, by AGN-blown cavities inflated in the surrounding X-ray gas. Such cavities are routinely observed at low-to-intermediate redshifts with *Chandra* and *XMM-Newton*, providing powerful insights into the physics of AGN feedback. High spatial resolution is critical; at redshifts $z > 1.5$, these

cavities are expected to typically subtend only a few arcsec (Figure 11). AXIS will extend these measurements, for the first time, into the high-redshift regime.

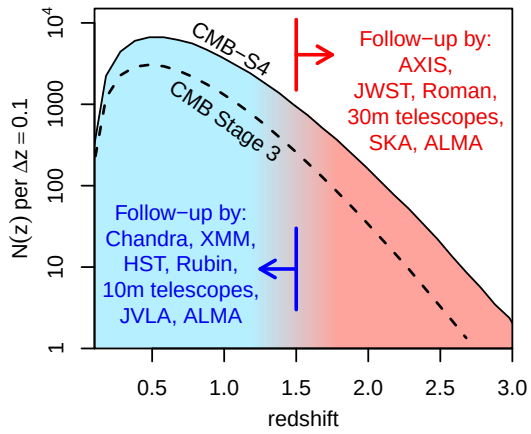

Figure 10. The number of SZ cluster detections expected as a function of redshift from Stage 3 SZ surveys and the proposed CMB-S4 project (adapted from [80]). Blue to red shading shows the transition to the $z > 1.5$ regime, for which high spatial resolution and throughput are key requirements for extracting information about halo centers, relative masses, dynamical states, internal structure, and galaxy/AGN populations.

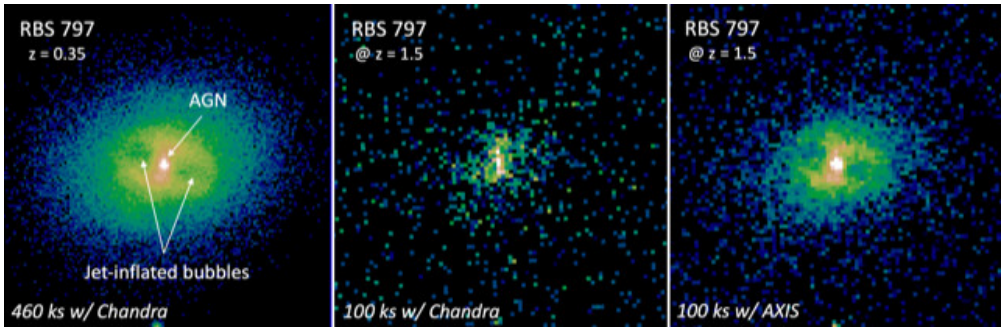

Figure 11. (**Left**): *Chandra* observation of the X-ray cavities in RBS 797. Two cavities are visible $\sim$ 30 kpc to the E and W of the AGN and are each $\sim$ 30 kpc across (e.g., [81]). (**Center**) and (**right**): *Chandra* and AXIS simulations of RBS 797 scaled for a mass of $M_{500} = 5 \times 10^{14}\,M_{\odot}$ at $z = 1.5$ (applying cosmological dimming, reducing angular size, etc.). AXIS will extend measurements of AGN feedback in these environments into the high redshift regime for the first time.

5.2. Metallicity Evolution

Measurements of cluster metallicity encode the entire history of star formation and AGN activity within cluster volumes, up to the redshift of observation, providing unique insights into the enrichment history of the universe. Metallicity distributions in clusters have been well characterized for nearby systems [82–84] and for statistical ensembles out to z$\sim$1.5 [85]. These reveal a remarkable universality from system to system and region to region within clusters [83,84], which requires that AGN feedback plays a profound role in redistributing metals throughout the universe at early times [86–88]. However, current X-ray flagship observatories lack the capability to perform such measurements at the redshifts most critical for evolutionary studies, $1.5 < z < 3.0$, when star formation and AGN activity in the universe peaked.

In order to probe high redshifts, including the period of cosmic noon ($2 < z < 3$), where we expect these processes to have been most prolific, we require spatially resolved X-ray measurements of clusters at these redshifts. As discussed in Section 5.1, Sunyaev-Zel'dovich (SZ) surveys, from SPT, ACT, the Simons Observatory and CMB-S4, will soon unveil, for the first time, the most massive, virialized systems at these redshifts, which will

be prime targets for X-ray followup with AXIS. Despite being the most massive structures in the universe, most of the extended emission from clusters at these redshifts is concentrated within regions less than an arcminute in size ($\sim r_{500}$). To simultaneously explore the physics of ongoing feedback within cluster cores, and the low surface brightness emission from cluster outskirts, while excising the emission from contaminating point sources, we require an instrument combining high sensitivity, high spatial resolution, and low particle background contamination. Only AXIS provides this combination.

The proposed 3 Ms AXIS observing program for 30 clusters at $1.5 < z < 3$ will transform our understanding of metal enrichment at high z, providing precise measurements for individual systems and tracing the evolutionary history of cluster enrichment as a whole. In combination with >20 Ms of existing X-ray observations from *Suzaku*, *Chandra*, and *XMM-Newton* at lower redshifts, the new AXIS measurements will provide the first meaningful constraints on the enrichment of the ICM at early times. The data will distinguish, to high precision, models in which enrichment in clusters tracks the star formation rate in the field, from models in which enrichment in the densest environments proceeds at an accelerated pace (as hinted at by recent studies with HST [89] and JWST [90]).

Figure 12 shows the existing constraints on the metallicity of cluster outskirts ($0.3 < r/r_{500} < 1.0$) from *Suzaku*, *Chandra* and *XMM-Newton*, binned in redshift, and the predicted measurements from 3 Ms of AXIS data (100 ks for each of the 30 clusters, divided equally among redshifts 1.5, 2.0, and 3.0). The baseline model assumed in the AXIS simulations (dashed line) is one where the enrichment of the ICM follows the same functional form as the cumulative star formation in field galaxies [27], i.e., metals are produced (and immediately dispersed) in cluster environments at the same rate, per unit mass, as in the field. An additional free parameter then allows the enrichment of cluster environments to be slowed or sped up relative to the field; slowing could result from the AGN feedback being delayed relative to star formation, while speedups may follow if star formation in the densest environments proceeds earlier than in the field. Although current data already disfavor significantly delayed enrichment in cluster environments, they remain consistent with arbitrarily rapid enrichment at early times, including models with approximately constant metallicity at all observable redshifts. In contrast, the addition of AXIS measurements will provide tight constraints, at the <10% level, on the rate of enrichment at early times, and a new anchor for studies of star formation and metal enrichment at high redshifts.

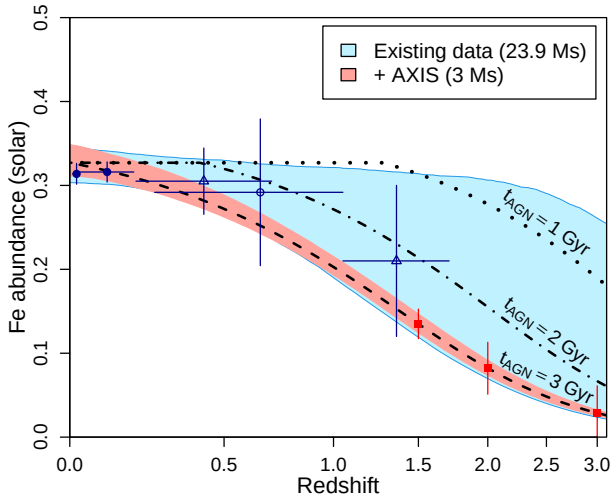

Figure 12. The forecasted improvement in metallicity constraints for cluster outskirts with AXIS. Current measurements (dark blue points) provide relatively weak constraints on how rapidly enrichment may have advanced in dense cluster environments, remaining consistent with even non-evolving metallicity (light blue band). The addition of 3 Ms of targeted AXIS data at $1.5 < z < 3$ will provide tight constraints on the rate of enrichment at early times, easily distinguishing between models where

the enrichment in dense cluster environments tracks the star formation rate in the field (red points and band), and models where the enrichment of denser environments proceeds faster (dotted and dash-dotted lines). t_{AGN} labels refer to the age of the universe when the rate of ICM enrichment is most rapid in each model.

6. The Circumgalactic Medium and Connections to the Cosmic Web

6.1. Connections to the Cosmic Web

The cosmic web forms the backbone of gas flows on cosmological scales. In the local universe, around half of all baryons are expected to lie in the Warm-Hot Intergalactic Medium (WHIM), $10^5 < T < 10^7$ K. The hottest part of the WHIM ($10^6 < T < 10^7$ K) can be revealed in the soft X-ray band (see [91,92] for reviews). However, due to its very low density, it is very faint in X-ray emission (see Figure 13). Only with a combination of a large effective area and low background can we observe the cosmic web in emission in X-rays. By combining with X-ray and UV absorption line studies from future missions, AXIS will enable a complete census of the baryons and metals in the local universe for the first time [93]. Cosmological simulations provide predictions for the distribution of metals in the cosmic web and how this distribution depends on AGN feedback over time. AXIS will test these models by charting the distribution of metals in the cluster outskirts and in the WHIM filaments. AXIS will also detect the missing baryons in the CGM around galaxies.

By measuring gas densities and temperatures in the outskirts of galaxy clusters, we will be able to measure the hydrostatic masses of clusters. Simulations predict that the contribution from non-thermal pressure support should increase in the outskirts, reaching a level of 10–30% of the total pressure, and by providing extra support against gravity. Comparing hydrostatic masses with gravitational lensing masses from Euclid and Roman will allow powerful constraints on the levels of non-thermal pressure support in the outskirts of clusters, where they interface with the cosmic web (e.g., [92]).

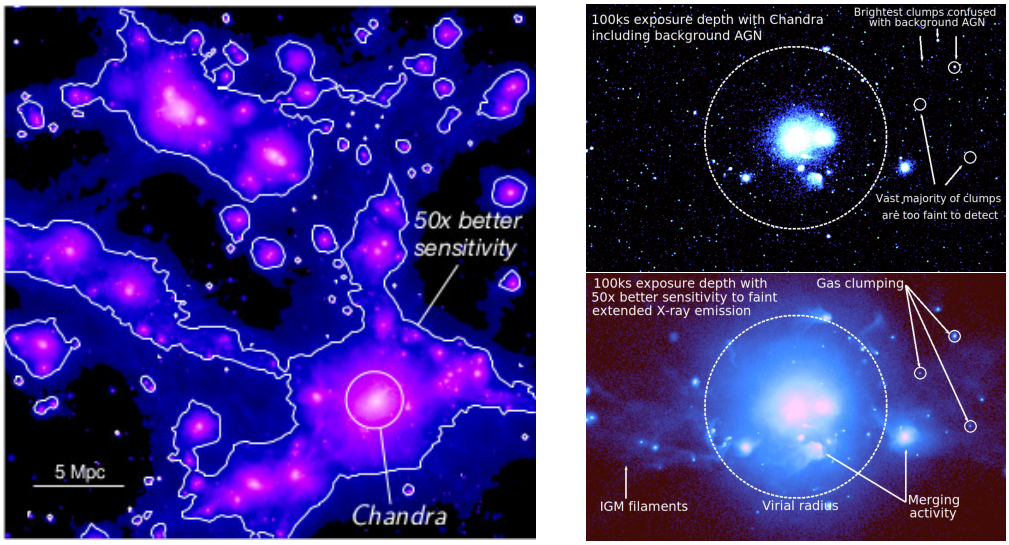

Figure 13. Left: Hydrodynamical cosmological simulation of large-scale structure formation, showing that galaxy clusters reside at the nodes of IGM filaments [94]. With *Chandra* and *XMM-Newton*, only the central regions of clusters can be explored in detail (inner white circle). To begin exploring a large-scale structure in its entirety (outer white contours) requires an improvement of at least a factor of 50 in sensitivity to low surface brightness extended emission. AXIS will achieve this increase in sensitivity through a combination of a high effective area and a low and stable particle background. Right: Simulated X-ray mosaic of the RomulusC cluster [95], a low mass (10^{14} $M_\odot$) cluster at $z = 0.05$, comparing 100 ks deep coverage from *Chandra* (top) and AXIS (bottom). The mock *Chandra* simulation includes background point sources from the cosmic X-ray background. Due to the high background

and small collecting areas of current X-ray telescopes, we are only able to see the brightest X-ray emission in the cluster cores. The bulk of the ICM in the outskirts beyond the virial radius (dashed white circle), and the IGM filaments that connect clusters together remain hidden from view. Figure adapted from [6].

The high spatial resolution of AXIS, along with its large effective area and low background compared to *Chandra*, would allow it to directly resolve and remove small-scale gas clumps and measure diffuse emission out to $\sim 2r_{200}$ (corresponding to around 2 Mpc for low mass clusters and 5 Mpc for the most massive clusters). Gas clumping is believed to be due to infalling gas substructures. Simulations indicate that the level of gas clumping should increase dramatically in the $(1–2)r_{200}$ region of clusters, where the infalling clumps have not yet been entirely ram-pressure stripped by the ICM [96–98]. If not resolved, clumping will bias gas profile measurements by overestimating the gas density and the gas mass fraction and underestimating the gas temperature, leading to biases in hydrostatic mass estimates [99,100]. Detecting and resolving gas clumps, which are associated with infalling galaxies in the outskirts of clusters, is also crucial to gain insight into the stripping of their CGM through their interactions with the ICM [101]. Removing gas clumps is critical in order to provide the strongest constraints on electron–ion equilibration and non-equilibrium ionization models in the outskirts of clusters (see Section 6.3 and [102–105]). Current X-ray telescopes are unable to resolve faint gas clumps that contribute to the bulk of the clumping (Figure 13, right), and their physical properties are almost completely unexplored.

6.2. Inflows and Outflows from Galaxy Clusters

Galaxy clusters are assembled through smooth accretion and occasional mergers of small structures (e.g., galaxies and groups) from the cosmic web (see [76,106] for reviews). The newly accreted IGM (i.e., inflows) is heated by accretion shocks at the boundary of the ICM and piles up in the cluster outskirts [107]. Mergers, on the other hand, not only stir cluster cores but also drive outflows that can significantly expand the hot atmosphere. It is crucial to study these inflow and outflow processes, not only to gain a deeper understanding of the hierarchical structure formation theory but also to leverage galaxy clusters as powerful tools to investigate cosmology and plasma physics.

Sharp gaseous structures, including shocks and contact discontinuities (for a review, see [108]), provide rich information on inflows and outflows of the ICM, e.g., their formation mechanisms, energy transportation, and dissipation. Current X-ray detections, performed by, for example, *Chandra* and *XMM-Newton*, are typically limited to within R_{500}. Zhang et al. [109,110] present a general picture of gaseous structures in the cluster outskirts, highlighting the significance of resolving discontinuities outside R_{500} to understand the dynamics of galaxy clusters (see Figure 1 in [110] for a sketch). Bow shocks formed ahead of infalling subhalos eventually detach from subhalos themselves after the primary core passages, occurring typically between R_{500} and R_{200}, and propagate all the way to the cluster peripheries [111]. The collisionless nature of these "runaway" shocks makes them ideal targets to characterize the electron–ion non-equilibrium and constrain the plasma physics of the ICM. Given the typical merger rate of galaxy clusters (e.g., [112]) and a combination of high spatial resolution and large effective area, AXIS is expected to detect a large number of such shocks. Together with radio surveys, we will be able to connect X-ray shocks with large-scale radio relics and understand how shocks with moderate Mach numbers accelerate electrons (see [113,114] for reviews).

The evolution of runaway shocks largely depends on the steepness of the gas density radial profiles for the diffuse ICM [111]. AXIS will provide an unprecedented measurement out to $2R_{200}$ by carefully excluding contributions from cold gas clumps (e.g., Figure 13). This is essential to understand the evolution of merger-driven outflows, e.g., the fate of runaway shocks, and how dramatically they can perturb/re-distribute matter and energy in the cluster outskirts.

Current theoretical studies predict that runaway shocks can be long-lived and eventually overtake accretion shocks and shape a new boundary of the ICM (i.e., merger-

accelerated accretion shock fronts or MA-shocks; see [109]), leading to a significant radial offset between the ICM and dark-matter halo boundaries. This is one of the most prominent effects caused by merger-driven outflows. Cosmological simulations show that the boundaries of the ICM (e.g., accretion shock fronts) are up to 5–6R_{200} in the non-filamentary directions (e.g., [115,116]). Detecting the Mpc-scale contact discontinuity near the virial radius formed together with the MA-shock can provide direct evidence of the merger-driven outflow and how it breaks ICM self-similarity in the cluster outskirts [110]. One such candidate has been tentatively identified in the Perseus cluster from deep *XMM-Newton* observations [117]. AXIS will not only provide detailed structures of the discontinuity interfaces (e.g., instabilities, mixing) but also extend the sample size, allowing a systematic study of the gas dynamics in the cluster outskirts.

Last but not least, along the filamentary directions, gas dynamics can be very different from the other diffuse directions, due to the anisotropy of the mass accretion rate [118]. Deeply penetrated filaments in the intracluster medium have been measured in cosmological simulations (e.g., [119]) and result in accretion shocks near and even within R_{200}. AXIS will be able to detect these innermost accretion shocks and characterize their role in thermalizing IGM and quenching infalling galaxies along the filaments.

6.3. Microphysics of the Intracluster and Circumgalactic Medium

The ICM and CGM are massive reservoirs of dilute, optically thin, weakly collisional (electrons and ions not necessarily in thermal equilibrium by Coulomb collisions), magnetized (with thermal to magnetic pressure > 100), and hot ($\sim 10^5 - 10^7$ K) plasmas which are ideal testbeds for microphysical transport processes (e.g., [120,121]). Since AXIS will allow the census and mapping of hot plasma out to the cluster/halo virial radius (see Section 6.1), energy transport across large volumes of these astrophysical environments can be studied. Cosmological hydrodynamic galaxy formation simulations apply phenomenological "sub-grid" prescriptions (e.g., [122,123]) for AGN feedback at the galactic scale. These models are not informed by the underlying physical transport and thermalization mechanisms. Thus, there is no good way to constrain how the diffuse plasma is heated and maintained despite an overall consensus on the source of energy. Moreover, this limits our understanding of how much multi-phase gas forms in the ICM/CGM—a key unknown of AGN feedback models (Sections 4.1 and 4.2). Although the magnetic field permeating the diffuse plasma is weak, its dynamical role is highlighted in fully collisionless models of the plasma (e.g., [124]) and more recently in magnetohydrodynamics ([125]). In the presence of typical magnetic fields and large-scale gradients of macroscopic variables (like density, temperature, etc.), a host of microinstabilities are generated at the electron/ion Larmor scale. These instabilities (e.g., whistlers/mirror/firehose) can grow to large amplitudes and scatter off electrons in the nonlinear stage to alter transport properties in weakly magnetized plasma (e.g., [126]). While the impact of this phenomenon at global scale is not widely explored (but see [127,128]) even in theoretical/computational research due to the large separation of scales, the consequences for AGN energy transport can be profound. The other aspect of energetics that is not explored sufficiently is the dissipation mechanism (kinetic to thermal energy conversion). Dissipation is crucial to combat the rapid cooling via free-free emission, especially in clusters. Overall, it is invaluable to experimentally measure these key plasma properties like electron–ion equilibration, energy transport, dissipation, role of magnetic field, etc., to prescribe accurate "sub-grid" computational models.

AXIS will be instrumental in analyzing shock discontinuity and contact discontinuity (in terms of electron temperature and density; see [108]) to assess the impact of plasma physics at macroscopic scales. First, the ratio of electron to ion temperature (e.g., [102]) behind the shock front is dependent on the Coulomb collisional timescale and plasma turbulence (which can transfer energy between the species). Very deep *Chandra* observations of a few of the brightest merger shocks have not produced a consensus on the equilibration timescale and mechanism from the electron temperature structure (Figure 14, see [129–131]). The large effective area of AXIS will allow us to map the detailed temperature structure

in the key region close to the shock front where equilibration models can be effectively distinguished. Secondly, the contact discontinuity ("cold front") will be smeared if the Kelvin–Helmholtz instability is strong at the interface (not viscous). Weakly compressible wave features will be sharp if energy transport and viscous dissipation processes are inefficient in the cluster plasma and their presence/absence can be verified by AXIS [132]. Moreover, an assessment of the survival timescale of jet-inflated bubbles can probe the levels of viscosity. Third, the electron temperature gradient maps can provide information on electron-dominated conduction [133], especially across shock fronts. Smaller gradients and/or an electron temperature precursor (electron temperature gradually increases from pre-shock to post-shock region) near a shock discontinuity will imply efficient transport. These investigations can be enabled via the combination of the high spatial resolution and large effective area of AXIS to obtain high signal-to-noise data on the scale of the electron mean-free path.

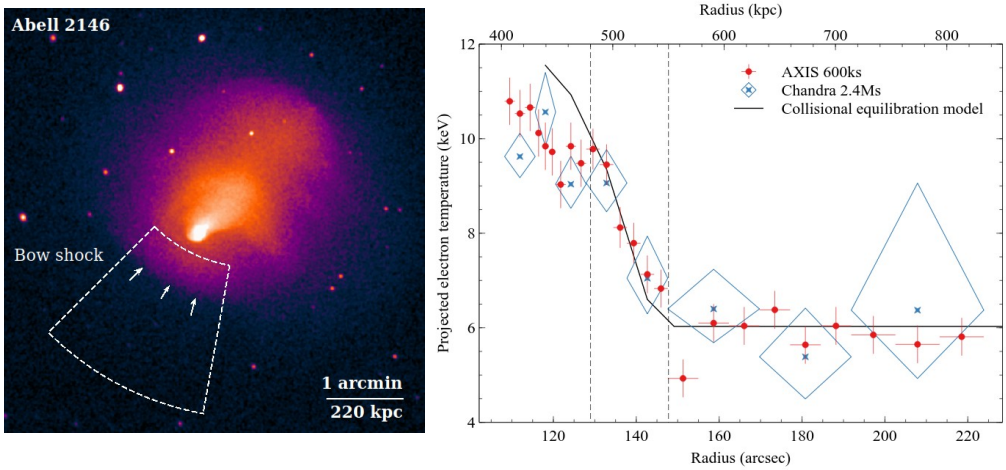

Figure 14. Left: *Chandra* image of the merging galaxy cluster Abell 2146 [129]. Right: Projected electron temperature profiles extracted for the sector across the bow shock front at a radius of ∼150 arcsec (shown on the left). The electrons are not directly heated by the shock front and instead come back into thermal equilibrium with the shock-heated ions behind the shock. The expectation for the collisional heating timescale is shown by the blue line. However, systematic uncertainties increasingly dominate with the distance behind the shock (shown by the low temperatures at radii <130 arcsec compared to the collisional model). AXIS will resolve the critical region of the post-shock gas (between the dashed lines), where equilibration models can be effectively distinguished.

7. Formation and Evolution of Large-Scale Structure

7.1. IGM Heating by Early X-ray Sources

Current and upcoming facilities are primed to peer back to the earliest cosmic epochs. JWST is now observing galaxies during the epoch of reionization (EoR), and 21 cm interferometers such as the Hydrogen Epoch of Reionziation (HERA) array will soon be sensitive to signals as far back as $z \sim 27$ [134]. The cosmic 21 cm signal is a window into the ionization state and thermal history of the intergalactic medium (IGM), which is sensitive to the high-energy (UV-to-X-ray) photons from the first galaxies (e.g., [135]). In particular, the X-ray emission from the first galaxies can both ionize and heat the neutral IGM, given the X-ray photons' longer mean free path. However, the timing of the X-ray heating in the early universe depends critically on assumptions about the sources of high-energy photons in early galaxies (e.g., [136]).

Recent theoretical models (e.g., [137,138]) predict that compact luminous accreting *stellar mass* objects (i.e., X-ray binaries, XRBs) would have dominated the X-ray emissivity at redshifts $z > 5$, leading to an epoch of heating (EoH) that precedes the EoR. However, predictions for X-ray heating at $z > 10$ from star-forming galaxies are based on extrapolations of X-ray emissivity trends that are constrained only at $z < 3$, a regime where

galaxies with actively accreting central engines dominate X-ray emissivity. For XRB emission from star-forming galaxies, the deepest existing survey fields yield direct detections in the hundreds of galaxies out to $z \sim 1$, with further measurements of XRB radiative power only out to $z \sim 3$, using high signal-to-noise stacks [139]. Therefore, we currently lack direct measurements of when XRBs begin to dominate the X-ray emissivity, limiting our understanding of the role of XRB feedback during key epochs in cosmic history, such as the EoH. AXIS, with its broad bandpass, high spatial resolution that is well matched to current and future facilities at other wavelengths, stable PSF across the FOV, and high effective area, will directly measure the X-ray emission from star-forming galaxies out to $z \sim 6-8$. With the nominal AXIS deep survey field, detections of XRB emission from star-forming galaxies will number in the thousands per redshift bin, providing a direct measurement of the redshift evolution of XRB emissivity. In this way, AXIS will bridge the gap between the locally measured XRB power output and upcoming indirect measurements of X-ray emission from the first galaxies at $z > 10$ from 21 cm interferometers.

7.2. Protocluster Structure

The large-scale environment is expected to have a major influence on galaxy evolution, particularly in so-called protoclusters [140]). These are defined as overdense regions on scales of several physical Mpc at $z > 2$ and are destined to evolve into galaxy clusters with masses in the range $10^{14} - 10^{15} M_{\odot}$ by $z = 0$ [141]. Gravitational processes, coupled with the larger availability of diffuse gas at higher densities and a high merger rate, are expected to drive enhanced star formation and a higher AGN duty cycle in protocluster galaxies, significantly affecting their evolution. In addition, according to the hierarchical model of structure formation, a few halos may be already virialized within the protocluster, heating the diffuse baryons and lighting up the proto-intra-cluster medium (proto-ICM) in the emission in the X-ray band.

Many of these aspects were recently highlighted in a deep *Chandra* observation of the archetypal Spiderweb protocluster [142], where a high AGN fraction of $25 \pm 5\%$ (corresponding to an enhancement of ~ 6 with respect to the COSMOS field) was measured in members with $\log(M_*) > 10.5$. The current measurement of the X-ray AGN fraction in protoclusters provides a confusing picture (see [142–144]), presumably obscured by the diversity of the large-scale structure investigated so far. With AXIS, we will routinely probe luminosities below $L_{[2-10\ \mathrm{keV}]} 10^{43}$ erg s^{-1} and measure the intrinsic absorption, iron line properties, and spectral slope in most of the protocluster AGN. AXIS will thereby reveal whether the X-ray nuclear emission is triggered by mergers, gas infall, or secular processes, and ultimately constrain the AGN duty cycle as a function of the local overdensity, redshift, and stellar mass of the host. In addition, the interactions of X-ray-emitting AGN and the warm diffuse baryons across the entire proto-ICM may explain the presence of large Lyα emission-line nebulae extending across several hundreds of kpc that have been recently discovered at high-z with integral-field unit spectrographs [145,146].

Another key scientific topic is the formation and evolution of the proto-ICM. Thanks to *Chandra*, a roughly spherical ICM halo with $kT \sim 2$ keV has been found around the Spiderweb Galaxy (see Figure 13 in [147]), clearly showing that all unresolved and diffuse components can be identified and characterized with $\sim$ arcsec angular resolution, even in the most complex case, where thermal and non-thermal emission largely overlap due to the presence of a bright radio galaxy. Coupling high angular resolution to the large effective area of AXIS, particularly at soft energies, will revolutionize protocluster studies in every aspect. In medium-deep exposures (of the order of 200–300 ks) with AXIS, the combination of imaging and spectral analysis will allow us to measure the chemical enrichment of the proto-ICM, the presence of temperature gradients, and possibly cooling flows (that can host much larger mass deposition rates compared to those at low redshifts), and the presence of cavities carved within the proto-ICM by mechanical feedback. In Figure 15, we compare the *Chandra* spectrum of the Spiderweb to that expected from a 200 ks exposure with AXIS at the aimpoint, finding that we can measure the average proto-ICM temperature with an

accuracy of 0.1 keV and the proto-ICM chemical abundance with an uncertainty of 20% for a reference case with an average temperature below 2 keV and an average metallicity of $0.3Z_{\odot}$ at $z \sim 2$.

Many other fields of investigation are made possible by AXIS. The spectral characterization of the non-thermal, diffuse X-ray emission from radio jets due to inverse Compton scattering onto the photons of the cosmic microwave background (and possibly local IR photons), allows us to directly constrain the magnetic fields and pressure around the jets, shedding light on the interactions between the relativistic electrons and the diffuse ICM (see [148,149]). In addition, with the high spatial resolution of AXIS, it will be possible to investigate the X-ray emission from a star formation in a single, strong starburst, and as an average across protocluster galaxies. Considering that a star formation rate of $100\,M_{\odot}\ yr^{-1}$ corresponds to $\sim 3 \times 10^{-17}$ erg cm^{-2} s^{-1} at $z = 2.5$, and that the cumulative SFR integrated over the protocluster members can amount to several thousands, the X-ray emission from star formation can be detected through stacking down to an average level of a few $M_{\odot}\ yr^{-1}$ over a population of ~ 100 protocluster members. In this way, AXIS will map the SFR from the central regions to the outskirts and constrain the triggering mechanisms of star formation episodes in protoclusters (see [150]). Finally, the hot ICM in virialized halos at temperatures above 1 keV can be serendipitously detected at any distance, considering that the typical surface brightness of virialized halos does not decrease significantly with redshift [151]. For the faintest halos, for which an X-ray spectral analysis is not viable, it is possible to recover the temperature and the entropy profiles by exploiting the complementarity of SZ and X-ray observations as demonstrated in the Spiderweb protocluster ([152], Lepore et al., in preparation).

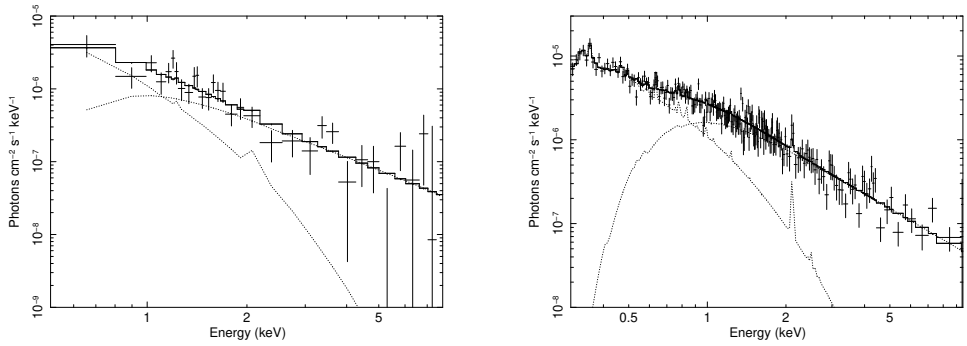

Figure 15. (**Left**): The *Chandra* spectrum (unfolded) of the thermal emission from the Spiderweb Galaxy halo within 12 arcsec removing the AGN and jets, from the entire exposure of 715 ks. Solid lines show the best fit obtained with a thermal `mekal` model plus the AGN contamination. (**Right**): The unfolded spectrum of this target from a simulated 200 ks AXIS observation at the aimpoint. To account for the larger PSF, the AGN contamination is twice that of the *Chandra* spectrum.

The study of the formation, evolution, and physical properties of protoclusters is one of the most vibrant fields in modern astrophysics and is rapidly advancing with new state-of-the-art instrumentation, such as JWST, ALMA, and MUSE@VLT. Furthermore, future survey missions, such as Euclid and the Vera Rubin Observatory, will prioritize the study of protoclusters. In the near future, these facilities will boost the number of known and well-characterized protoclusters, providing a large sample of large-scale overdensities across different epochs, with vastly different properties.

8. Conclusions

AXIS will be a powerful community-based X-ray observatory for the 2030s. The unparalleled combination of arcsecond spatial resolution, high throughput, and wide field of view will allow AXIS to capture the complete picture of feedback from the impact zones, where stellar winds, AGN winds, and radio jets collide with the ISM, to the widespread distribu-

tion of energy and metal-rich gas across galaxy and cluster halos. The low instrumental background and wide field of view of AXIS will finally permit a dramatic emergence of the cosmic web as a vast network of soft X-ray filaments, reveal the establishment of feedback in clusters at cosmic noon, and show us the structure of the first groups and clusters at high redshift. The primary science goals of AXIS on galaxy evolution and feedback address the science questions asked by the Astro2020 Decadal 'Cosmic Ecosystems' priority area and, as such, will have a wide-ranging impact on the whole astronomical community. From radio jets (ngVLA, SKA) and the multi-phase gas flows driven by feedback in galaxies and clusters (ELT/TMT, JWST, ALMA) to the detection of massive clusters at high redshift (CMB-S4, Simons Observatory, Rubin, Roman and Euclid), AXIS has synergies with essentially every planned observatory for the 2030s. Companion white papers on topics including stellar physics and exoplanets, compact object populations and supernova remnants, transients and multi-messenger astronomy, and the evolution of AGN demonstrate the breadth of discoveries that the AXIS probe mission will deliver for the entire astronomical community.

Author Contributions: H.R.R. and L.A.L.: conceptualization, analysis, writing, review and editing. L.A.L., M.Y., E.H.-K. and K.G. contributed Section 2. A.T.-F., H.R.R., F.T. and W.P.M. contributed Section 3.1. G.C. contributed Section 3.2. L.L. and H.R.R. contributed Section 4.1. Y.Q. contributed Section 4.2. A.C.F. contributed Sections 4.3 and 4.4. S.W.A., A.B.M. and M.M. contributed Section 5.1. A.M.F., A.B.M. and S.W.A. contributed Section 5.2. S.A.W. and K.-W.W. contributed Section Section 6.1. C.Z. contributed Section 6.2. P.P.C. and C.S.R. contributed Section 6.3. K.G. and B.D.L. contributed Section 7.1. P.T. contributed Section 7.2. R.A.D., M.J.K., J.-T.L., E.D.M., R.F.M.: writing original draft; writing review & editing. All authors have read and agreed to the published version of the manuscript.

Funding: The authors declare that financial support was received for the research, authorship, and publication of this article. HRR acknowledges funding from an STFC Ernest Rutherford Fellowship and an Anne McLaren Fellowship from the University of Nottingham. LAL acknowledges support by the Heising-Simons Foundation and the Simons Foundation. This work was performed in part at the Simons Foundation Flatiron Institute's Center for Computational Astrophysics during L.A.L.'s time as an IDEA Scholar.

Data Availability Statement: Raw and processed data products detailed in this paper will be made available on reasonable request to the author.

Acknowledgments: We thank everyone who has contributed to the development of the AXIS Probe mission concept. We thank the reviewers for their helpful comments.

Conflicts of Interest: The authors declare that the research was conducted in the absence of any commercial or financial relationships that could be construed as potential conflicts of interest.

References

1. Wechsler, R.H.; Tinker, J.L. The Connection Between Galaxies and Their Dark Matter Halos. *Annu. Rev. Astron. Astrophys.* **2018**, *56*, 435–487. https://doi.org/10.1146/annurev-astro-081817-051756.
2. Veilleux, S.; Cecil, G.; Bland-Hawthorn, J. Galactic Winds. *Annu. Rev. Astron. Astrophys.* **2005**, *43*, 769–826. https://doi.org/10.1146/annurev.astro.43.072103.150610.
3. Heckman, T.M.; Thompson, T.A. Galactic Winds and the Role Played by Massive Stars. In *Handbook of Supernovae*; Alsabti, A.W., Murdin, P., Eds.; Springer: Berlin/Heidelberg, Germany, 2017; p. 2431. https://doi.org/10.1007/978-3-319-21846-5_23.
4. Fabian, A.C. Observational Evidence of Active Galactic Nuclei Feedback. *Annu. Rev. Astron. Astrophys.* **2012**, *50*, 455–489. https://doi.org/10.1146/annurev-astro-081811-125521.
5. Reynolds, C.S.; Kara, E.A.; Mushotzky, R.F.; Ptak, A.; Koss, M.J.; Williams, B.J.; Allen, S.W.; Bauer, F.E.; Bautz, M.; Bodaghee, A.; et al. Overview of the Advanced X-ray Imaging Satellite (AXIS). *SPIE* **2023**, *12678*, 12678E. https://doi.org/10.1117/12.2677468.
6. Walker, S.; Nagai, D.; Simionescu, A.; Markevitch, M.; Akamatsu, H.; Arnaud, M.; Avestruz, C.; Bautz, M.; Biffi, V.; Borgani, S.; et al. Unveiling the Galaxy Cluster - Cosmic Web Connection with X-ray observations in the Next Decade. *Bull. Am. Astron. Soc.* **2019**, *51*, 218. https://doi.org/10.48550/arXiv.1903.04550.
7. Hopkins, P.F.; Kereš, D.; Oñorbe, J.; Faucher-Giguère, C.A.; Quataert, E.; Murray, N.; Bullock, J.S. Galaxies on FIRE (Feedback In Realistic Environments): Stellar feedback explains cosmologically inefficient star formation. *Mon. Not. R. Astron. Soc.* **2014**, *445*, 581–603. https://doi.org/10.1093/mnras/stu1738.

8. Chevance, M.; Kruijssen, J.M.D.; Hygate, A.P.S.; Schruba, A.; Longmore, S.N.; Groves, B.; Henshaw, J.D.; Herrera, C.N.; Hughes, A.; Jeffreson, S.M.R.; et al. The lifecycle of molecular clouds in nearby star-forming disc galaxies. *Mon. Not. R. Astron. Soc.* **2020**, *493*, 2872–2909. https://doi.org/10.1093/mnras/stz3525.
9. Krumholz, M.R.; McKee, C.F.; Bland-Hawthorn, J. Star Clusters Across Cosmic Time. *Annu. Rev. Astron. Astrophys.* **2019**, *57*, 227–303. https://doi.org/10.1146/annurev-astro-091918-104430.
10. Dobbs, C.L.; Krumholz, M.R.; Ballesteros-Paredes, J.; Bolatto, A.D.; Fukui, Y.; Heyer, M.; Low, M.M.M.; Ostriker, E.C.; Vázquez-Semadeni, E. Formation of Molecular Clouds and Global Conditions for Star Formation. *Protostars Planets VI* **2014**, 3–26. https://doi.org/10.2458/azu_uapress_9780816531240-ch001.
11. Rosen, A.L.; Lopez, L.A.; Krumholz, M.R.; Ramirez-Ruiz, E. Gone with the wind: Where is the missing stellar wind energy from massive star clusters? *Mon. Not. R. Astron. Soc.* **2014**, *442*, 2701–2716. https://doi.org/10.1093/mnras/stu1037.
12. Lancaster, L.; Ostriker, E.C.; Kim, J.G.; Kim, C.G. Efficiently Cooled Stellar Wind Bubbles in Turbulent Clouds. I. Fractal Theory and Application to Star-forming Clouds. *Astrophys. J.* **2021**, *914*, 89. https://doi.org/10.3847/1538-4357/abf8ab.
13. McNamara, B.R.; Nulsen, P.E.J. Mechanical feedback from active galactic nuclei in galaxies, groups and clusters. *New J. Phys.* **2012**, *14*, 055023. https://doi.org/10.1088/1367-2630/14/5/055023.
14. Magorrian, J.; Tremaine, S.; Richstone, D.; Bender, R.; Bower, G.; Dressler, A.; Faber, S.M.; Gebhardt, K.; Green, R.; Grillmair, C.; et al. The Demography of Massive Dark Objects in Galaxy Centers. *Astrophys. J.* **1998**, *115*, 2285–2305. https://doi.org/10.1086/300353.
15. Bower, R.G.; Benson, A.J.; Malbon, R.; Helly, J.C.; Frenk, C.S.; Baugh, C.M.; Cole, S.; Lacey, C.G. Breaking the hierarchy of galaxy formation. *Mon. Not. R. Astron. Soc.* **2006**, *370*, 645–655. https://doi.org/10.1111/j.1365-2966.2006.10519.x.
16. Croton, D.J.; Springel, V.; White, S.D.M.; De Lucia, G.; Frenk, C.S.; Gao, L.; Jenkins, A.; Kauffmann, G.; Navarro, J.F.; Yoshida, N. The many lives of active galactic nuclei: Cooling flows, black holes and the luminosities and colours of galaxies. *Mon. Not. R. Astron. Soc.* **2006**, *365*, 11–28. https://doi.org/10.1111/j.1365-2966.2005.09675.x.
17. Silk, J.; Rees, M.J. Quasars and galaxy formation. *Astron. Astrophys.* **1998**, *331*, L1–L4. https://doi.org/10.48550/arXiv.astro-ph/9801013.
18. Fabian, A.C. The obscured growth of massive black holes. *Mon. Not. R. Astron. Soc.* **1999**, *308*, L39–L43. https://doi.org/10.1046/j.1365-8711.1999.03017.x.
19. King, A. Black Holes, Galaxy Formation, and the M_{BH}-σ Relation. *Astrophys. J.* **2003**, *596*, L27–L29. https://doi.org/10.1086/379143.
20. Murray, N.; Quataert, E.; Thompson, T.A. On the Maximum Luminosity of Galaxies and Their Central Black Holes: Feedback from Momentum-driven Winds. *Astrophys. J.* **2005**, *618*, 569–585. https://doi.org/10.1086/426067.
21. Fabbiano, G.; Paggi, A.; Karovska, M.; Elvis, M.; Maksym, W.P.; Risaliti, G.; Wang, J. Deep Chandra Observations of ESO 428-G014. II. Spectral Properties and Morphology of the Large-scale Extended X-ray Emission. *Astrophys. J.* **2018**, *855*, 131. https://doi.org/10.3847/1538-4357/aab1f4.
22. Maksym, W.P.; Fabbiano, G.; Elvis, M.; Karovska, M.; Paggi, A.; Raymond, J.; Wang, J.; Storchi-Bergmann, T.; Risaliti, G. CHEERS Results from NGC 3393. III. Chandra X-Ray Spectroscopy of the Narrow Line Region. *Astrophys. J.* **2019**, *872*, 94. https://doi.org/10.3847/1538-4357/aaf4f5.
23. Trindade Falcao, A.; Fabbiano, G.; Elvis, M.; Paggi, A.; Maksym, W.P. Deep Chandra Observations of NGC 5728: Morphology and Spectral Properties of the Extended X-Ray Emission. *Astrophys. J.* **2023**, *950*, 143. https://doi.org/10.3847/1538-4357/acd052.
24. Fornasini, F.M.; Elvis, M.; Maksym, W.P.; Fabbiano, G.; Bergmann, T.S.; Gandhi, P.; Whittle, M. Termination Shocks and the Extended X-Ray Emission in Mrk 78. *Astrophys. J.* **2022**, *931*, 65. https://doi.org/10.3847/1538-4357/ac694d.
25. King, A.; Pounds, K. Powerful Outflows and Feedback from Active Galactic Nuclei. *Annu. Rev. Astron. Astrophys.* **2015**, *53*, 115–154. https://doi.org/10.1146/annurev-astro-082214-122316.
26. Paggi, A.; Wang, J.; Fabbiano, G.; Elvis, M.; Karovska, M. CHEERS Results on Mrk 573: A Study of Deep Chandra Observations. *Astrophys. J.* **2012**, *756*, 39. https://doi.org/10.1088/0004-637X/756/1/39.
27. Madau, P.; Dickinson, M. Cosmic Star-Formation History . *Annu. Rev. Astron. Astrophys.* **2014**, *52*, 415–486. https://doi.org/10.1146/annurev-astro-081811-125615.
28. Faucher-Giguère, C.A.; Quataert, E. The physics of galactic winds driven by active galactic nuclei. *Mon. Not. R. Astron. Soc.* **2012**, *425*, 605–622. https://doi.org/10.1111/j.1365-2966.2012.21512.x.
29. Zubovas, K.; King, A. Clearing Out a Galaxy. *Astrophys. J.* **2012**, *745*, L34. https://doi.org/10.1088/2041-8205/745/2/L34.
30. Kochanek, C.S.; Keeton, C.R.; McLeod, B.A. The Importance of Einstein Rings. *Astrophys. J.* **2001**, *547*, 50–59. https://doi.org/10.1086/318350.
31. Chartas, G.; Cappi, M.; Vignali, C.; Dadina, M.; James, V.; Lanzuisi, G.; Giustini, M.; Gaspari, M.; Strickland, S.; Bertola, E. Multiphase Powerful Outflows Detected in High-z Quasars. *Astrophys. J.* **2021**, *920*, 24. https://doi.org/10.3847/1538-4357/ac0ef2.
32. Chartas, G.; Cappi, M.; Vignali, C.; Dadina, M.; Giustini, M.; Lanzuisi, G.; Gaspari, M.; Bertola, E. Quasar Winds and their Interaction with the ISM at High-z. *Bull. Am. Astron. Soc.* **2023**, *55*, 300.01.
33. Oguri, M. The image separation distribution of strong lenses: Halo versus subhalo populations. *Mon. Not. R. Astron. Soc.* **2006**, *367*, 1241–1250. https://doi.org/10.1111/j.1365-2966.2006.10043.x.

34. McNamara, B.R.; Nulsen, P.E.J. Heating Hot Atmospheres with Active Galactic Nuclei. *Annu. Rev. Astron. Astrophys.* **2007**, *45*, 117–175. https://doi.org/10.1146/annurev.astro.45.051806.110625.
35. Ogle, P.M.; Lanz, L.; Appleton, P.N. Jet-shocked H_2 and CO in the Anomalous Arms of Molecular Hydrogen Emission Galaxy NGC 4258. *Astrophys. J.* **2014**, *788*, L33. https://doi.org/10.1088/2041-8205/788/2/L33.
36. Lanz, L.; Ogle, P.M.; Evans, D.; Appleton, P.N.; Guillard, P.; Emonts, B. Jet-ISM Interaction in the Radio Galaxy 3C 293: Jet-driven Shocks Heat ISM to Power X-Ray and Molecular H_2 Emission. *Astrophys. J.* **2015**, *801*, 17. https://doi.org/10.1088/0004-637X/801/1/17.
37. Werner, N.; McNamara, B.R.; Churazov, E.; Scannapieco, E. Hot Atmospheres, Cold Gas, AGN Feedback and the Evolution of Early Type Galaxies: A Topical Perspective. Space Sci. Rew. **2019**, *215*, 5. https://doi.org/10.1007/s11214-018-0571-9.
38. McNamara, B.R.; Wise, M.; Nulsen, P.E.J.; David, L.P.; Sarazin, C.L.; Bautz, M.; Markevitch, M.; Vikhlinin, A.; Forman, W.R.; Jones, C.; et al. Chandra X-Ray Observations of the Hydra A Cluster: An Interaction between the Radio Source and the X-Ray-emitting Gas. *Astrophys. J.* **2000**, *534*, L135–L138. https://doi.org/10.1086/312662.
39. Fabian, A.C.; Sanders, J.S.; Ettori, S.; Taylor, G.B.; Allen, S.W.; Crawford, C.S.; Iwasawa, K.; Johnstone, R.M.; Ogle, P.M. Chandra imaging of the complex X-ray core of the Perseus cluster. *Mon. Not. R. Astron. Soc.* **2000**, *318*, L65–L68. https://doi.org/10.1046/j.1365-8711.2000.03904.x.
40. Churazov, E.; Brüggen, M.; Kaiser, C.R.; Böhringer, H.; Forman, W. Evolution of Buoyant Bubbles in M87. *Astrophys. J.* **2001**, *554*, 261–273. https://doi.org/10.1086/321357.
41. Forman, W.; Jones, C.; Churazov, E.; Markevitch, M.; Nulsen, P.; Vikhlinin, A.; Begelman, M.; Böhringer, H.; Eilek, J.; Heinz, S.; et al. Filaments, Bubbles, and Weak Shocks in the Gaseous Atmosphere of M87. *Astrophys. J.* **2007**, *665*, 1057–1066. https://doi.org/10.1086/519480.
42. Sanders, J.S.; Fabian, A.C.; Taylor, G.B.; Russell, H.R.; Blundell, K.M.; Canning, R.E.A.; Hlavacek-Larrondo, J.; Walker, S.A.; Grimes, C.K. A very deep Chandra view of metals, sloshing and feedback in the Centaurus cluster of galaxies. *Mon. Not. R. Astron. Soc.* **2016**, *457*, 82–109. https://doi.org/10.1093/mnras/stv2972.
43. Blanton, E.L.; Randall, S.W.; Douglass, E.M.; Sarazin, C.L.; Clarke, T.E.; McNamara, B.R. Shocks and Bubbles in a Deep Chandra Observation of the Cooling Flow Cluster Abell 2052. *Astrophys. J.* **2009**, *697*, L95–L98. https://doi.org/10.1088/0004-637X/697/2/L95.
44. Nulsen, P.; Jones, C.; Forman, W.; Churazov, E.; McNamara, B.; David, L.; Murray, S. Radio Mode Outbursts in Giant Elliptical Galaxies. In *The Monster's Fiery Breath: Feedback in Galaxies, Groups, and Clusters*; Heinz, S., Wilcots, E., Eds.; American Institute of Physics Conference Series; American Institute of Physics: College Park, MD, USA, 2009; Volume 1201; pp. 198–201. https://doi.org/10.1063/1.3293033.
45. Shin, J.; Woo, J.H.; Mulchaey, J.S. A Systematic Search for X-Ray Cavities in Galaxy Clusters, Groups, and Elliptical Galaxies. *Astrophys. J. Suppl. Ser.* **2016**, *227*, 31. https://doi.org/10.3847/1538-4365/227/2/31.
46. Kim, D.W.; Fabbiano, G. X-Ray Scaling Relations of 'Core' and 'Coreless' E and S0 Galaxies. *Astrophys. J.* **2015**, *812*, 127. https://doi.org/10.1088/0004-637X/812/2/127.
47. Cappellari, M.; Emsellem, E.; Krajnović, D.; McDermid, R.M.; Scott, N.; Verdoes Kleijn, G.A.; Young, L.M.; Alatalo, K.; Bacon, R.; Blitz, L.; et al. The ATLAS^{3D} project - I. A volume-limited sample of 260 nearby early-type galaxies: Science goals and selection criteria. *Mon. Not. R. Astron. Soc.* **2011**, *413*, 813–836. https://doi.org/10.1111/j.1365-2966.2010.18174.x.
48. Nyland, K.; Young, L.M.; Wrobel, J.M.; Sarzi, M.; Morganti, R.; Alatalo, K.; Blitz, L.; Bournaud, F.; Bureau, M.; Cappellari, M.; et al. The ATLAS^{3D} Project - XXXI. Nuclear radio emission in nearby early-type galaxies. *Mon. Not. R. Astron. Soc.* **2016**, *458*, 2221–2268. https://doi.org/10.1093/mnras/stw391.
49. Das, S.; Mathur, S.; Gupta, A.; Nicastro, F.; Krongold, Y. Multiple Temperature Components of the Hot Circumgalactic Medium of the Milky Way. *Astrophys. J.* **2019**, *887*, 257. https://doi.org/10.3847/1538-4357/ab5846.
50. Sanders, J.S. Contour binning: A new technique for spatially resolved X-ray spectroscopy applied to Cassiopeia A. *Mon. Not. R. Astron. Soc.* **2006**, *371*, 829–842. https://doi.org/10.1111/j.1365-2966.2006.10716.x.
51. Randall, S.W.; Forman, W.R.; Giacintucci, S.; Nulsen, P.E.J.; Sun, M.; Jones, C.; Churazov, E.; David, L.P.; Kraft, R.; Donahue, M.; et al. Shocks and Cavities from Multiple Outbursts in the Galaxy Group NGC 5813: A Window to Active Galactic Nucleus Feedback. *Astrophys. J.* **2011**, *726*, 86. https://doi.org/10.1088/0004-637X/726/2/86.
52. Randall, S.W.; Nulsen, P.E.J.; Jones, C.; Forman, W.R.; Bulbul, E.; Clarke, T.E.; Kraft, R.; Blanton, E.L.; David, L.; Werner, N.; et al. A Very Deep Chandra Observation of the Galaxy Group NGC 5813: AGN Shocks, Feedback, and Outburst History. *Astrophys. J.* **2015**, *805*, 112. https://doi.org/10.1088/0004-637X/805/2/112.
53. Bîrzan, L.; Rafferty, D.A.; McNamara, B.R.; Wise, M.W.; Nulsen, P.E.J. A Systematic Study of Radio-induced X-Ray Cavities in Clusters, Groups, and Galaxies. *Astrophys. J.* **2004**, *607*, 800–809 https://doi.org/10.1086/383519.
54. Li, Y.; Bryan, G.L.; Ruszkowski, M.; Voit, G.M.; O'Shea, B.W.; Donahue, M. Cooling, AGN Feedback, and Star Formation in Simulated Cool-core Galaxy Clusters. *Astrophys. J.* **2015**, *811*, 73. https://doi.org/10.1088/0004-637X/811/2/73.
55. Qiu, Y.; Bogdanović, T.; Li, Y.; McDonald, M. Using Hα Filaments to Probe Active Galactic Nuclei Feedback in Galaxy Clusters. *Astrophys. J. Lett.* **2019**, *872*, L11. https://doi.org/10.3847/2041-8213/ab0375.
56. Pizzolato, F.; Soker, N. On the Nature of Feedback Heating in Cooling Flow Clusters. *Astrophys. J.* **2005**, *632*, 821–830. https://doi.org/10.1086/444344.

57. Gaspari, M.; Ruszkowski, M.; Sharma, P. Cause and Effect of Feedback: Multiphase Gas in Cluster Cores Heated by AGN Jets. *Astrophys. J.* **2012**, *746*, 94. https://doi.org/10.1088/0004-637X/746/1/94.
58. Li, Y.; Bryan, G.L. Modeling Active Galactic Nucleus Feedback in Cool-core Clusters: The Formation of Cold Clumps. *Astrophys. J.* **2014**, *789*, 153. https://doi.org/10.1088/0004-637X/789/2/153.
59. McNamara, B.R.; Russell, H.R.; Nulsen, P.E.J.; Hogan, M.T.; Fabian, A.C.; Pulido, F.; Edge, A.C. A Mechanism for Stimulating AGN Feedback by Lifting Gas in Massive Galaxies. *Astrophys. J.* **2016**, *830*, 79. https://doi.org/10.3847/0004-637X/830/2/79.
60. Voit, G.M.; Meece, G.; Li, Y.; O'Shea, B.W.; Bryan, G.L.; Donahue, M. A Global Model for Circumgalactic and Cluster-core Precipitation. *Astrophys. J.* **2017**, *845*, 80. https://doi.org/10.3847/1538-4357/aa7d04.
61. Qiu, Y.; Bogdanović, T.; Li, Y.; McDonald, M.; McNamara, B.R. The formation of dusty cold gas filaments from galaxy cluster simulations. *Nat. Astron.* **2020**, *4*, 900–906. https://doi.org/10.1038/s41550-020-1090-7.
62. Li, Y.; Gendron-Marsolais, M.L.; Zhuravleva, I.; Xu, S.; Simionescu, A.; Tremblay, G.R.; Lochhaas, C.; Bryan, G.L.; Quataert, E.; Murray, N.W.; et al. Direct Detection of Black Hole-driven Turbulence in the Centers of Galaxy Clusters. *Astrophys. J. Lett.* **2020**, *889*, L1. https://doi.org/10.3847/2041-8213/ab65c7.
63. Zhang, C.; Zhuravleva, I.; Gendron-Marsolais, M.L.; Churazov, E.; Schekochihin, A.A.; Forman, W.R. Bubble-driven gas uplift in galaxy clusters and its velocity features. *Mon. Not. R. Astron. Soc.* **2022**, *517*, 616–631. https://doi.org/10.1093/mnras/stac2282.
64. Fabian, A.C.; Sanders, J.S.; Williams, R.J.R.; Lazarian, A.; Ferland, G.J.; Johnstone, R.M. The energy source of the filaments around the giant galaxy NGC 1275. *Mon. Not. R. Astron. Soc.* **2011**, *417*, 172–177. https://doi.org/10.1111/j.1365-2966.2011.19034.x.
65. Voit, G.M.; Kay, S.T.; Bryan, G.L. The baseline intracluster entropy profile from gravitational structure formation. *Mon. Not. R. Astron. Soc.* **2005**, *364*, 909–916. https://doi.org/10.1111/j.1365-2966.2005.09621.x.
66. Zhuravleva, I.; Churazov, E.; Schekochihin, A.A.; Allen, S.W.; Arévalo, P.; Fabian, A.C.; Forman, W.R.; Sanders, J.S.; Simionescu, A.; Sunyaev, R.; et al. Turbulent heating in galaxy clusters brightest in X-rays. *Nature* **2014**, *515*, 85–87. https://doi.org/10.1038/nature13830.
67. Peterson, J.R.; Paerels, F.B.S.; Kaastra, J.S.; Arnaud, M.; Reiprich, T.H.; Fabian, A.C.; Mushotzky, R.F.; Jernigan, J.G.; Sakelliou, I. X-ray imaging-spectroscopy of Abell 1835. *Astron. Astrophys.* **2001**, *365*, L104–L109. https://doi.org/10.1051/0004-6361:20000021.
68. Kaastra, J.S.; Ferrigno, C.; Tamura, T.; Paerels, F.B.S.; Peterson, J.R.; Mittaz, J.P.D. XMM-Newton observations of the cluster of galaxies Sérsic 159-03. *Astron. Astrophys.* **2001**, *365*, L99–L103. https://doi.org/10.1051/0004-6361:20000041.
69. Sanders, J.S.; Fabian, A.C.; Allen, S.W.; Morris, R.G.; Graham, J.; Johnstone, R.M. Cool X-ray emitting gas in the core of the Centaurus cluster of galaxies. *Mon. Not. R. Astron. Soc.* **2008**, *385*, 1186–1200. https://doi.org/10.1111/j.1365-2966.2008.12952.x.
70. Fabian, A.C.; Ferland, G.J.; Sanders, J.S.; McNamara, B.R.; Pinto, C.; Walker, S.A. Hidden cooling flows in clusters of galaxies. *Mon. Not. R. Astron. Soc.* **2022**, *515*, 3336–3345. https://doi.org/10.1093/mnras/stac2003.
71. Fabian, A.C.; Sanders, J.S.; Ferland, G.J.; McNamara, B.R.; Pinto, C.; Walker, S.A. Hidden Cooling Flows in Clusters of Galaxies III: Accretion onto the Central Black Hole. *Mon. Not. R. Astron. Soc.* **2023**, *524*, 716–730. https://doi.org/10.1093/mnras/stad1870.
72. Fabian, A.C.; Walker, S.A.; Russell, H.R.; Pinto, C.; Canning, R.E.A.; Salome, P.; Sanders, J.S.; Taylor, G.B.; Zweibel, E.G.; Conselice, C.J.; et al. HST imaging of the dusty filaments and nucleus swirl in NGC4696 at the centre of the Centaurus Cluster. *Mon. Not. R. Astron. Soc.* **2016**, *461*, 922–928. https://doi.org/10.1093/mnras/stw1350.
73. Fabian, A.C.; Chapman, S.; Casey, C.M.; Bauer, F.; Blundell, K.M. The extended X-ray emission around HDF130 at z = 1.99: An inverse Compton ghost of a giant radio source in the Chandra Deep Field-North. *Mon. Not. R. Astron. Soc.* **2009**, *395*, L67–L70. https://doi.org/10.1111/j.1745-3933.2009.00644.x.
74. Mocz, P.; Fabian, A.C.; Blundell, K.M. Inverse-Compton ghosts and double-lobed radio sources in the X-ray sky. *Mon. Not. R. Astron. Soc.* **2011**, *413*, 1107–1120. https://doi.org/10.1111/j.1365-2966.2011.18198.x.
75. Allen, S.W.; Evrard, A.E.; Mantz, A.B. Cosmological Parameters from Observations of Galaxy Clusters. *Annu. Rev. Astron. Astrophys.* **2011**, *49*, 409–470. https://doi.org/10.1146/annurev-astro-081710-102514.
76. Kravtsov, A.V.; Borgani, S. Formation of Galaxy Clusters. *Annu. Rev. Astron. Astrophys.* **2012**, *50*, 353–409. https://doi.org/10.1146/annurev-astro-081811-125502.
77. McDonald, M.; Allen, S.W.; Bayliss, M.; Benson, B.A.; Bleem, L.E.; Brodwin, M.; Bulbul, E.; Carlstrom, J.E.; Forman, W.R.; Hlavacek-Larrondo, J.; et al. The Remarkable Similarity of Massive Galaxy Clusters from z $\sim$ 0 to z $\sim$ 1.9. *Astrophys. J.* **2017**, *843*, 28. https://doi.org/10.3847/1538-4357/aa7740.
78. Sanders, J.S.; Fabian, A.C.; Russell, H.R.; Walker, S.A. Hydrostatic Chandra X-ray analysis of SPT-selected galaxy clusters - I. Evolution of profiles and core properties. *Mon. Not. R. Astron. Soc.* **2018**, *474*, 1065–1098 https://doi.org/10.1093/mnras/stx2796.
79. Ghirardini, V.; Bulbul, E.; Kraft, R.; Bayliss, M.; Benson, B.; Bleem, L.; Bocquet, S.; Calzadilla, M.; Eckert, D.; Forman, W.; et al. Evolution of the Thermodynamic Properties of Clusters of Galaxies out to Redshift of 1.8. *Astrophys. J.* **2021**, *910*, 14. https://doi.org/10.3847/1538-4357/abc68d.
80. Mantz, A.; Allen, S.W.; Battaglia, N.; Benson, B.; Canning, R.; Ettori, S.; Evrard, A.; von der Linden, A.; McDonald, M.; Abidi, M.; et al. The Future Landscape of High-Redshift Galaxy Cluster Science. *Bull. Am. Astron. Soc.* **2019**, *51*, 279. https://doi.org/10.48550/arXiv.1903.05606.
81. Ubertosi, F.; Gitti, M.; Brighenti, F.; Brunetti, G.; McDonald, M.; Nulsen, P.; McNamara, B.; Randall, S.; Forman, W.; Donahue, M.; et al. The Deepest Chandra View of RBS 797: Evidence for Two Pairs of Equidistant X-ray Cavities. *Astrophys. J. Lett.* **2021**, *923*, L25. https://doi.org/10.3847/2041-8213/ac374c.

82. de Grandi, S.; Molendi, S. Metal abundances in the cool cores of galaxy clusters. *Astron. Astrophys.* **2009**, *508*, 565–574. https://doi.org/10.1051/0004-6361/200912745.
83. Werner, N.; Urban, O.; Simionescu, A.; Allen, S.W. A uniform metal distribution in the intergalactic medium of the Perseus cluster of galaxies. *Nature* **2013**, *502*, 656–658. https://doi.org/10.1038/nature12646.
84. Urban, O.; Werner, N.; Allen, S.W.; Simionescu, A.; Mantz, A. A uniform metallicity in the outskirts of massive, nearby galaxy clusters. *Mon. Not. R. Astron. Soc.* **2017**, *470*, 4583–4599. https://doi.org/10.1093/mnras/stx1542.
85. Flores, A.M.; Mantz, A.B.; Allen, S.W.; Morris, R.G.; Canning, R.E.A.; Bleem, L.E.; Calzadilla, M.S.; Floyd, B.T.; McDonald, M.; Ruppin, F. The history of metal enrichment traced by X-ray observations of high-redshift galaxy clusters. *Mon. Not. R. Astron. Soc.* **2021**, *507*, 5195–5204. https://doi.org/10.1093/mnras/stab2430.
86. Biffi, V.; Planelles, S.; Borgani, S.; Fabjan, D.; Rasia, E.; Murante, G.; Tornatore, L.; Dolag, K.; Granato, G.L.; Gaspari, M.; et al. The history of chemical enrichment in the intracluster medium from cosmological simulations. *Mon. Not. R. Astron. Soc.* **2017**, *468*, 531–548. https://doi.org/10.1093/mnras/stx444.
87. Biffi, V.; Planelles, S.; Borgani, S.; Rasia, E.; Murante, G.; Fabjan, D.; Gaspari, M. The origin of ICM enrichment in the outskirts of present-day galaxy clusters from cosmological hydrodynamical simulations. *Mon. Not. R. Astron. Soc.* **2018**, *476*, 2689–2703. https://doi.org/10.1093/mnras/sty363.
88. Vogelsberger, M.; Marinacci, F.; Torrey, P.; Genel, S.; Springel, V.; Weinberger, R.; Pakmor, R.; Hernquist, L.; Naiman, J.; Pillepich, A.; et al. The uniformity and time-invariance of the intra-cluster metal distribution in galaxy clusters from the IllustrisTNG simulations. *Mon. Not. R. Astron. Soc.* **2018**, *474*, 2073–2093. https://doi.org/10.1093/mnras/stx2955.
89. Willis, J.P.; Canning, R.E.A.; Noordeh, E.S.; Allen, S.W.; King, A.L.; Mantz, A.; Morris, R.G.; Stanford, S.A.; Brammer, G. Spectroscopic confirmation of a mature galaxy cluster at a redshift of 2. *Nature* **2020**, *577*, 39–41. https://doi.org/10.1038/s41586-019-1829-4.
90. Tacchella, S.; Eisenstein, D.J.; Hainline, K.; Johnson, B.D.; Baker, W.M.; Helton, J.M.; Robertson, B.; Suess, K.A.; Chen, Z.; Nelson, E.; et al. JADES Imaging of GN-z11: Revealing the Morphology and Environment of a Luminous Galaxy 430 Myr after the Big Bang. *Astrophys. J.* **2023**, *952*, 74. https://doi.org/10.3847/1538-4357/acdbc6.
91. Reiprich, T.H.; Basu, K.; Ettori, S.; Israel, H.; Lovisari, L.; Molendi, S.; Pointecouteau, E.; Roncarelli, M. Outskirts of Galaxy Clusters. *Space Sci. Rev.* **2013**, *177*, 195–245. https://doi.org/10.1007/s11214-013-9983-8.
92. Walker, S.; Simionescu, A.; Nagai, D.; Okabe, N.; Eckert, D.; Mroczkowski, T.; Akamatsu, H.; Ettori, S.; Ghirardini, V. The Physics of Galaxy Cluster Outskirts. *Space Sci. Rev.* **2019**, *215*, 7. https://doi.org/10.1007/s11214-018-0572-8.
93. Richter, P.; Paerels, F.B.S.; Kaastra, J.S. FUV and X-Ray Absorption in the Warm-Hot Intergalactic Medium. *Space Sci. Rev.* **2008**, *134*, 25–49. https://doi.org/10.1007/s11214-008-9325-4.
94. Dolag, K.; Meneghetti, M.; Moscardini, L.; Rasia, E.; Bonaldi, A. Simulating the physical properties of dark matter and gas inside the cosmic web. *Mon. Not. R. Astron. Soc.* **2006**, *370*, 656–672. https://doi.org/10.1111/j.1365-2966.2006.10511.x.
95. Tremmel, M.; Quinn, T.R.; Ricarte, A.; Babul, A.; Chadayammuri, U.; Natarajan, P.; Nagai, D.; Pontzen, A.; Volonteri, M. Introducing ROMULUSC: A cosmological simulation of a galaxy cluster with an unprecedented resolution. *Mon. Not. R. Astron. Soc.* **2019**, *483*, 3336–3362. https://doi.org/10.1093/mnras/sty3336.
96. Nagai, D.; Lau, E.T. Gas Clumping in the Outskirts of ΛCDM Clusters. *Astrophys. J. Lett.* **2011**, *731*, L10. https://doi.org/10.1088/2041-8205/731/1/L10.
97. Roncarelli, M.; Ettori, S.; Borgani, S.; Dolag, K.; Fabjan, D.; Moscardini, L. Large-scale inhomogeneities of the intracluster medium: Improving mass estimates using the observed azimuthal scatter. *Mon. Not. R. Astron. Soc.* **2013**, *432*, 3030–3046. https://doi.org/10.1093/mnras/stt654.
98. Vazza, F.; Eckert, D.; Simionescu, A.; Brüggen, M.; Ettori, S. Properties of gas clumps and gas clumping factor in the intra-cluster medium. *Mon. Not. R. Astron. Soc.* **2013**, *429*, 799–814. https://doi.org/10.1093/mnras/sts375.
99. Simionescu, A.; Allen, S.W.; Mantz, A.; Werner, N.; Takei, Y.; Morris, R.G.; Fabian, A.C.; Sanders, J.S.; Nulsen, P.E.J.; George, M.R.; et al. Baryons at the Edge of the X-ray-Brightest Galaxy Cluster. *Science* **2011**, *331*, 1576. https://doi.org/10.1126/science.1200331.
100. Towler, I.; Kay, S.T.; Altamura, E. Gas clumping and its effect on hydrostatic bias in the MACSIS simulations. *Mon. Not. R. Astron. Soc.* **2023**, *520*, 5845–5857. https://doi.org/10.1093/mnras/stad453.
101. Cen, R.; Pop, A.R.; Bahcall, N.A. Gas loss in simulated galaxies as they fall into clusters. *Proc. Natl. Acad. Sci. USA* **2014**, *111*, 7914–7919. https://doi.org/10.1073/pnas.1407300111.
102. Wong, K.W.; Sarazin, C.L. Effects of the Non-Equipartition of Electrons and Ions in the Outskirts of Relaxed Galaxy Clusters. *Astrophys. J.* **2009**, *707*, 1141–1159. https://doi.org/10.1088/0004-637X/707/2/1141.
103. Wong, K.W.; Sarazin, C.L.; Ji, L. X-ray Signatures of Non-equilibrium Ionization Effects in Galaxy Cluster Accretion Shock Regions. *Astrophys. J.* **2011**, *727*, 126. https://doi.org/10.1088/0004-637X/727/2/126.
104. Avestruz, C.; Nagai, D.; Lau, E.T.; Nelson, K. Non-equilibrium Electrons in the Outskirts of Galaxy Clusters. *Astrophys. J.* **2015**, *808*, 176. https://doi.org/10.1088/0004-637X/808/2/176.
105. Andreon, S.; Moretti, A.; Böhringer, H.; Castagna, F. The flat entropy profile at the outskirts of the Abell 2244 galaxy cluster. *Mon. Not. R. Astron. Soc.* **2023**, *519*, 2366–2374. https://doi.org/10.1093/mnras/stac3525.
106. Vikhlinin, A.A.; Kravtsov, A.V.; Markevich, M.L.; Sunyaev, R.A.; Churazov, E.M. Clusters of galaxies. *Phys. Uspekhi* **2014**, *57*, 317–341. https://doi.org/10.3367/UFNe.0184.201404a.0339.

107. Bertschinger, E. Self-similar secondary infall and accretion in an Einstein-de Sitter universe. *Astrophys. J. Suppl. Ser.* **1985**, *58*, 39–65. https://doi.org/10.1086/191028.
108. Markevitch, M.; Vikhlinin, A. Shocks and cold fronts in galaxy clusters. *Phys. Rep.* **2007**, *443*, 1–53. https://doi.org/10.1016/j.physrep.2007.01.001.
109. Zhang, C.; Churazov, E.; Dolag, K.; Forman, W.R.; Zhuravleva, I. Encounters of merger and accretion shocks in galaxy clusters and their effects on intracluster medium. *Mon. Not. R. Astron. Soc.* **2020**, *494*, 4539–4547. https://doi.org/10.1093/mnras/staa1013.
110. Zhang, C.; Churazov, E.; Dolag, K.; Forman, W.R.; Zhuravleva, I. Collision of merger and accretion shocks: Formation of Mpc-scale contact discontinuity in the Perseus cluster. *Mon. Not. R. Astron. Soc.* **2020**, *498*, L130–L134. https://doi.org/10.1093/mnrasl/slaa147.
111. Zhang, C.; Churazov, E.; Forman, W.R.; Lyskova, N. Runaway merger shocks in galaxy cluster outskirts and radio relics. *Mon. Not. R. Astron. Soc.* **2019**, *488*, 5259–5266. https://doi.org/10.1093/mnras/stz2135.
112. Fakhouri, O.; Ma, C.P.; Boylan-Kolchin, M. The merger rates and mass assembly histories of dark matter haloes in the two Millennium simulations. *Mon. Not. R. Astron. Soc.* **2010**, *406*, 2267–2278. https://doi.org/10.1111/j.1365-2966.2010.16859.x.
113. Bykov, A.M.; Vazza, F.; Kropotina, J.A.; Levenfish, K.P.; Paerels, F.B.S. Shocks and Non-thermal Particles in Clusters of Galaxies. *Space Sci. Rev.* **2019**, *215*, 14. https://doi.org/10.1007/s11214-019-0585-y.
114. van Weeren, R.J.; de Gasperin, F.; Akamatsu, H.; Brüggen, M.; Feretti, L.; Kang, H.; Stroe, A.; Zandanel, F. Diffuse Radio Emission from Galaxy Clusters. *Space Sci. Rev.* **2019**, *215*, 16. https://doi.org/10.1007/s11214-019-0584-z.
115. Lau, E.T.; Nagai, D.; Avestruz, C.; Nelson, K.; Vikhlinin, A. Mass Accretion and its Effects on the Self-similarity of Gas Profiles in the Outskirts of Galaxy Clusters. *Astrophys. J.* **2015**, *806*, 68. https://doi.org/10.1088/0004-637X/806/1/68.
116. Aung, H.; Nagai, D.; Lau, E.T. Shock and splash: Gas and dark matter halo boundaries around ΛCDM galaxy clusters. *Mon. Not. R. Astron. Soc.* **2021**, *508*, 2071–2078. https://doi.org/10.1093/mnras/stab2598.
117. Walker, S.A.; Mirakhor, M.S.; ZuHone, J.; Sanders, J.S.; Fabian, A.C.; Diwanji, P. Is There an Enormous Cold Front at the Virial Radius of the Perseus Cluster? *Astrophys. J.* **2022**, *929*, 37. https://doi.org/10.3847/1538-4357/ac5894.
118. Vurm, I.; Nevalainen, J.; Hong, S.E.; Bahé, Y.M.; Dalla Vecchia, C.; Heinämäki, P. Cosmic gas highways in C-EAGLE simulations. *Astron. Astrophys.* **2023**, *673*, A62. https://doi.org/10.1051/0004-6361/202243904.
119. Zinger, E.; Dekel, A.; Birnboim, Y.; Kravtsov, A.; Nagai, D. The role of penetrating gas streams in setting the dynamical state of galaxy clusters. *Mon. Not. R. Astron. Soc.* **2016**, *461*, 412–432. https://doi.org/10.1093/mnras/stw1283.
120. Helander, P.; Sigmar, D.J. *Collisional Transport in Magnetized Plasmas*; Cambridge University Press: Cambridge, UK, 2005; Volume 4.
121. Schekochihin, A.A.; Cowley, S.C.; Dorland, W.; Hammett, G.W.; Howes, G.G.; Quataert, E.; Tatsuno, T. Astrophysical Gyrokinetics: Kinetic and Fluid Turbulent Cascades in Magnetized Weakly Collisional Plasmas. *Astrophys. J.* **2009**, *182*, 310–377. https://doi.org/10.1088/0067-0049/182/1/310.
122. Vogelsberger, M.; Genel, S.; Sijacki, D.; Torrey, P.; Springel, V.; Hernquist, L. A model for cosmological simulations of galaxy formation physics. *Mon. Not. R. Astron. Soc.* **2013**, *436*, 3031–3067. https://doi.org/10.1093/mnras/stt1789.
123. Crain, R.A.; Schaye, J.; Bower, R.G.; Furlong, M.; Schaller, M.; Theuns, T.; Dalla Vecchia, C.; Frenk, C.S.; McCarthy, I.G.; Helly, J.C.; et al. The EAGLE simulations of galaxy formation: Calibration of subgrid physics and model variations. *Mon. Not. R. Astron. Soc.* **2015**, *450*, 1937–1961. https://doi.org/10.1093/mnras/stv725.
124. Komarov, S.V.; Churazov, E.M.; Kunz, M.W.; Schekochihin, A.A. Thermal conduction in a mirror-unstable plasma. *Mon. Not. R. Astron. Soc.* **2016**, *460*, 467–477. https://doi.org/10.1093/mnras/stw963.
125. Drake, J.F.; Pfrommer, C.; Reynolds, C.S.; Ruszkowski, M.; Swisdak, M.; Einarsson, A.; Thomas, T.; Hassam, A.B.; Roberg-Clark, G.T. Whistler-regulated Magnetohydrodynamics: Transport Equations for Electron Thermal Conduction in the High-β Intracluster Medium of Galaxy Clusters. *Astrophys. J.* **2021**, *923*, 245. https://doi.org/10.3847/1538-4357/ac1ff1.
126. Schekochihin, A.A.; Cowley, S.C.; Kulsrud, R.M.; Rosin, M.S.; Heinemann, T. Nonlinear Growth of Firehose and Mirror Fluctuations in Astrophysical Plasmas. *Phys. Rev. Lett.* **2008**, *100*, 081301. https://doi.org/10.1103/PhysRevLett.100.081301.
127. Berlok, T.; Quataert, E.; Pessah, M.E.; Pfrommer, C. Suppressed heat conductivity in the intracluster medium: implications for the magneto-thermal instability. *Mon. Not. R. Astron. Soc.* **2021**, *504*, 3435–3454. https://doi.org/10.1093/mnras/stab832.
128. Beckmann, R.S.; Dubois, Y.; Pellissier, A.; Polles, F.L.; Olivares, V. AGN jets do not prevent the suppression of conduction by the heat buoyancy instability in simulated galaxy clusters. *Astron. Astrophys.* **2022**, *666*, A71. https://doi.org/10.1051/0004-6361/202243873.
129. Russell, H.R.; Nulsen, P.E.J.; Caprioli, D.; Chadayammuri, U.; Fabian, A.C.; Kunz, M.W.; McNamara, B.R.; Sanders, J.S.; Richard-Laferrière, A.; Beleznay, M.; et al. The structure of cluster merger shocks: Turbulent width and the electron heating time-scale. *Mon. Not. R. Astron. Soc.* **2022**, *514*, 1477–1493. https://doi.org/10.1093/mnras/stac1055.
130. Markevitch, M. Chandra Observation of the Most Interesting Cluster in the Universe. In *The X-ray Universe 2005*; Wilson, A., Ed.; ESA Special Publication: Paris, France, 2006; Volume 604, p. 723. https://doi.org/10.48550/arXiv.astro-ph/0511345.
131. Wang, Q.H.S.; Giacintucci, S.; Markevitch, M. Bow Shock in Merging Cluster A520: The Edge of the Radio Halo and the Electron-Proton Equilibration Timescale. *Astrophys. J.* **2018**, *856*, 162. https://doi.org/10.3847/1538-4357/aab2aa.
132. Choudhury, P.P.; Reynolds, C.S. Acoustic waves and g-mode turbulence as energy carriers in a viscous intracluster medium. *Mon. Not. R. Astron. Soc.* **2022**, *514*, 3765–3788. https://doi.org/10.1093/mnras/stac1457.
133. Ettori, S.; Fabian, A.C. Chandra constraints on the thermal conduction in the intracluster plasma of A2142. *Mon. Not. R. Astron. Soc.* **2000**, *317*, L57–L59. https://doi.org/10.1046/j.1365-8711.2000.03899.x.

134. Abdurashidova, Z.; Aguirre, J.E.; Alexander, P.; Ali, Z.S.; Balfour, Y.; Beardsley, A.P.; Bernardi, G.; Billings, T.S.; Bowman, J.D.; Bradley, R.F.; et al. First Results from HERA Phase I: Upper Limits on the Epoch of Reionization 21 cm Power Spectrum. *Astrophys. J.* **2022**, *925*, 221, [arXiv:astro-ph.CO/2108.02263]. https://doi.org/10.3847/1538-4357/ac1c78.
135. McQuinn, M. The Evolution of the Intergalactic Medium. *Annu. Rev. Astron. Astrophys.* **2016**, *54*, 313–362. https://doi.org/10.1146/annurev-astro-082214-122355.
136. Mesinger, A.; Ferrara, A.; Spiegel, D.S. Signatures of X-rays in the early Universe. *Mon. Not. R. Astron. Soc.* **2013**, *431*, 621–637. https://doi.org/10.1093/mnras/stt198.
137. Fragos, T.; Lehmer, B.D.; Naoz, S.; Zezas, A.; Basu-Zych, A. Energy Feedback from X-Ray Binaries in the Early Universe. *Astrophys. J. Lett.* **2013**, *776*, L31. https://doi.org/10.1088/2041-8205/776/2/L31.
138. Madau, P.; Fragos, T. Radiation Backgrounds at Cosmic Dawn: X-Rays from Compact Binaries. *Astrophys. J.* **2017**, *840*, 39. https://doi.org/10.3847/1538-4357/aa6af9.
139. Lehmer, B.D.; Basu-Zych, A.R.; Mineo, S.; Brandt, W.N.; Eufrasio, R.T.; Fragos, T.; Hornschemeier, A.E.; Luo, B.; Xue, Y.Q.; Bauer, F.E.; et al. The Evolution of Normal Galaxy X-Ray Emission through Cosmic History: Constraints from the 6 MS Chandra Deep Field-South. *Astrophys. J.* **2016**, *825*, 7. https://doi.org/10.3847/0004-637X/825/1/7.
140. Overzier, R.A. The realm of the galaxy protoclusters. A review. *Astron. Astrophys. Rev.* **2016**, *24*, 14. https://doi.org/10.1007/s00159-016-0100-3.
141. Chiang, Y.K.; Overzier, R.; Gebhardt, K. Ancient Light from Young Cosmic Cities: Physical and Observational Signatures of Galaxy Proto-clusters. *Astrophys. J.* **2013**, *779*, 127. https://doi.org/10.1088/0004-637X/779/2/127.
142. Tozzi, P.; Pentericci, L.; Gilli, R.; Pannella, M.; Fiore, F.; Miley, G.; Nonino, M.; Röttgering, H.J.A.; Strazzullo, V.; Anderson, C.S.; et al. The 700 ks Chandra Spiderweb Field. I. Evidence for widespread nuclear activity in the protocluster. *Astron. Astrophys.* **2022**, *662*, A54. https://doi.org/10.1051/0004-6361/202142333.
143. Vito, F.; Brandt, W.N.; Lehmer, B.D.; Vignali, C.; Zou, F.; Bauer, F.E.; Bremer, M.; Gilli, R.; Ivison, R.J.; Spingola, C. Chandra reveals a luminous Compton-thick QSO powering a Lyα blob in a z = 4 starbursting protocluster. *Astron. Astrophys.* **2020**, *642*, A149. https://doi.org/10.1051/0004-6361/202038848.
144. Polletta, M.; Soucail, G.; Dole, H.; Lehnert, M.D.; Pointecouteau, E.; Vietri, G.; Scodeggio, M.; Montier, L.; Koyama, Y.; Lagache, G.; et al. Spectroscopic observations of PHz G237.01+42.50: A galaxy protocluster at z = 2.16 in the Cosmos field. *Astron. Astrophys.* **2021**, *654*, A121. https://doi.org/10.1051/0004-6361/202140612.
145. Cantalupo, S.; Arrigoni-Battaia, F.; Prochaska, J.X.; Hennawi, J.F.; Madau, P. A cosmic web filament revealed in Lyman-α emission around a luminous high-redshift quasar. *Nature* **2014**, *506*, 63–66. https://doi.org/10.1038/nature12898.
146. Arrigoni Battaia, F.; Chen, C.C.; Fumagalli, M.; Cai, Z.; Calistro Rivera, G.; Xu, J.; Smail, I.; Prochaska, J.X.; Yang, Y.; De Breuck, C. Overdensity of submillimeter galaxies around the z $\sim$ 2.3 MAMMOTH-1 nebula. The environment and powering of an enormous Lyman-α nebula. *Astron. Astrophys.* **2018**, *620*, A202. https://doi.org/10.1051/0004-6361/201834195.
147. Tozzi, P.; Gilli, R.; Liu, A.; Borgani, S.; Lepore, M.; Di Mascolo, L.; Saro, A.; Pentericci, L.; Carilli, C.; Miley, G.; et al. The 700 ks Chandra Spiderweb Field. II. Evidence for inverse-Compton and thermal diffuse emission in the Spiderweb galaxy. *Astron. Astrophys.* **2022**, *667*, A134. https://doi.org/10.1051/0004-6361/202244337.
148. Carilli, C.L.; Anderson, C.S.; Tozzi, P.; Pannella, M.; Clarke, T.; Pentericci, L.; Liu, A.; Mroczkowski, T.; Miley, G.K.; Rottgering, H.J.; et al. X-Ray Emission from the Jets and Lobes of the Spiderweb. *Astrophys. J.* **2022**, *928*, 59, [arXiv:astro-ph.HE/2203.03506]. https://doi.org/10.3847/1538-4357/ac55a0.
149. Anderson, C.S.; Carilli, C.L.; Tozzi, P.; Miley, G.K.; Borgani, S.; Clarke, T.; Di Mascolo, L.; Liu, A.; Mroczkowski, T.; Pannella, M.; et al. The Spiderweb Protocluster is Being Magnetized by Its Central Radio Jet. *Astrophys. J.* **2022**, *937*, 45. https://doi.org/10.3847/1538-4357/ac7ec0.
150. Chiang, Y.K.; Overzier, R.A.; Gebhardt, K.; Henriques, B. Galaxy Protoclusters as Drivers of Cosmic Star Formation History in the First 2 Gyr. *Astrophys. J. Lett.* **2017**, *844*, L23. https://doi.org/10.3847/2041-8213/aa7e7b.
151. Churazov, E.; Vikhlinin, A.; Sunyaev, R. (No) dimming of X-ray clusters beyond z $\sim$ 1 at fixed mass: Crude redshifts and masses from raw X-ray and SZ data. *Mon. Not. R. Astron. Soc.* **2015**, *450*, 1984–1989. https://doi.org/10.1093/mnras/stv743.
152. Di Mascolo, L.; Saro, A.; Mroczkowski, T.; Borgani, S.; Churazov, E.; Rasia, E.; Tozzi, P.; Dannerbauer, H.; Basu, K.; Carilli, C.L.; et al. Forming intracluster gas in a galaxy protocluster at a redshift of 2.16. *Nature* **2023**, *615*, 809–812, [arXiv:astro-ph.CO/2303.16226]. https://doi.org/10.1038/s41586-023-05761-x.